Dark Matter
In
Extreme Astrophysical Environments

TACOS 2023

Kuver Sinha
University of Oklahoma

Snowmass 2021

Submitted to the Proceedings of the US Community Study
on the Future of Particle Physics (Snowmass 2021)

Dark Matter In Extreme Astrophysical Environments

Masha Baryakhtar[1], Regina Caputo[2], Djuna Croon[3,4], Kerstin Perez[5], Emanuele Berti[6], Joseph Bramante[7,8], Malte Buschmann[9], Richard Brito[10], Thomas Y. Chen[11], Philippa S. Cole[12], Adam Coogan[13,14], William E. East[8], Joshua W. Foster[5], Marios Galanis[15], Maurizio Giannotti[16], Bradley J. Kavanagh[17], Ranjan Laha[18], Rebecca K. Leane[19,20], Benjamin V. Lehmann[21,22], Gustavo Marques-Tavares[23], Jamie McDonald[4,24], Ken K. Y. Ng[5,25], Nirmal Raj[26], Laura Sagunski[27], Jeremy Sakstein[28], B.S. Sathyaprakash[29,30,42,43], Sarah Shandera[29,30], Nils Siemonsen[7,8,31], Olivier Simon[14], Kuver Sinha[32], Divya Singh[29, 21], Rajeev Singh[33], Chen Sun[34], Ling Sun[35], Volodymyr Takhistov[36], Yu-Dai Tsai[37], Edoardo Vitagliano[38], Salvatore Vitale[5,24], Huan Yang[8,39], and Jun Zhang[40,41]

What Happened?

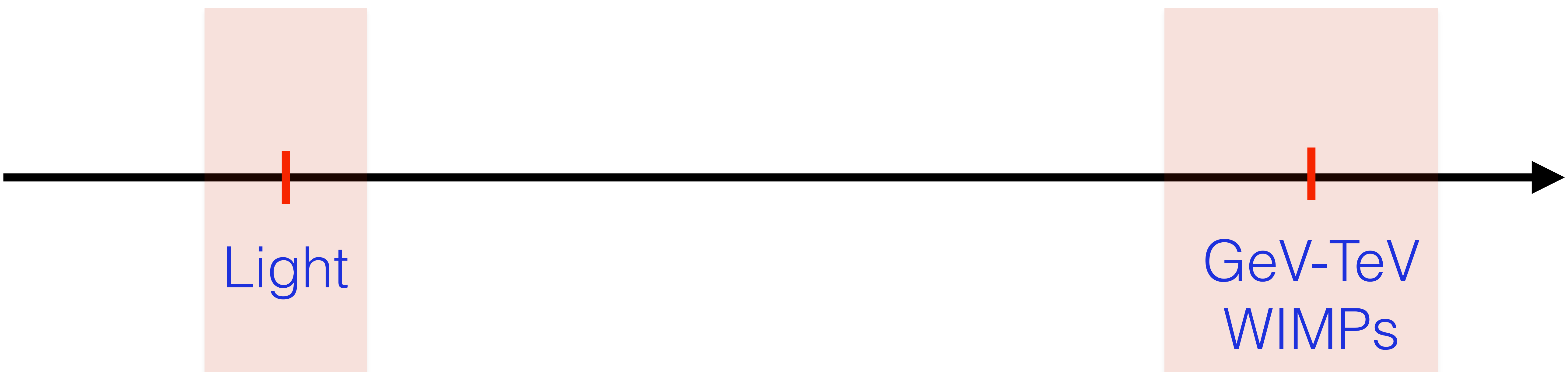

Supernovas
Neutron star mergers
Black holes
Magnetars
White Dwarfs

Colliders
Direct/ indirect detection

Why Extreme?

High temperatures

High densities

Large magnetic fields

Large gravitational fields

Radio, X-ray, Gamma -ray signals

Possibility of gravitational waves/multi messenger signals

Snowmass 2021

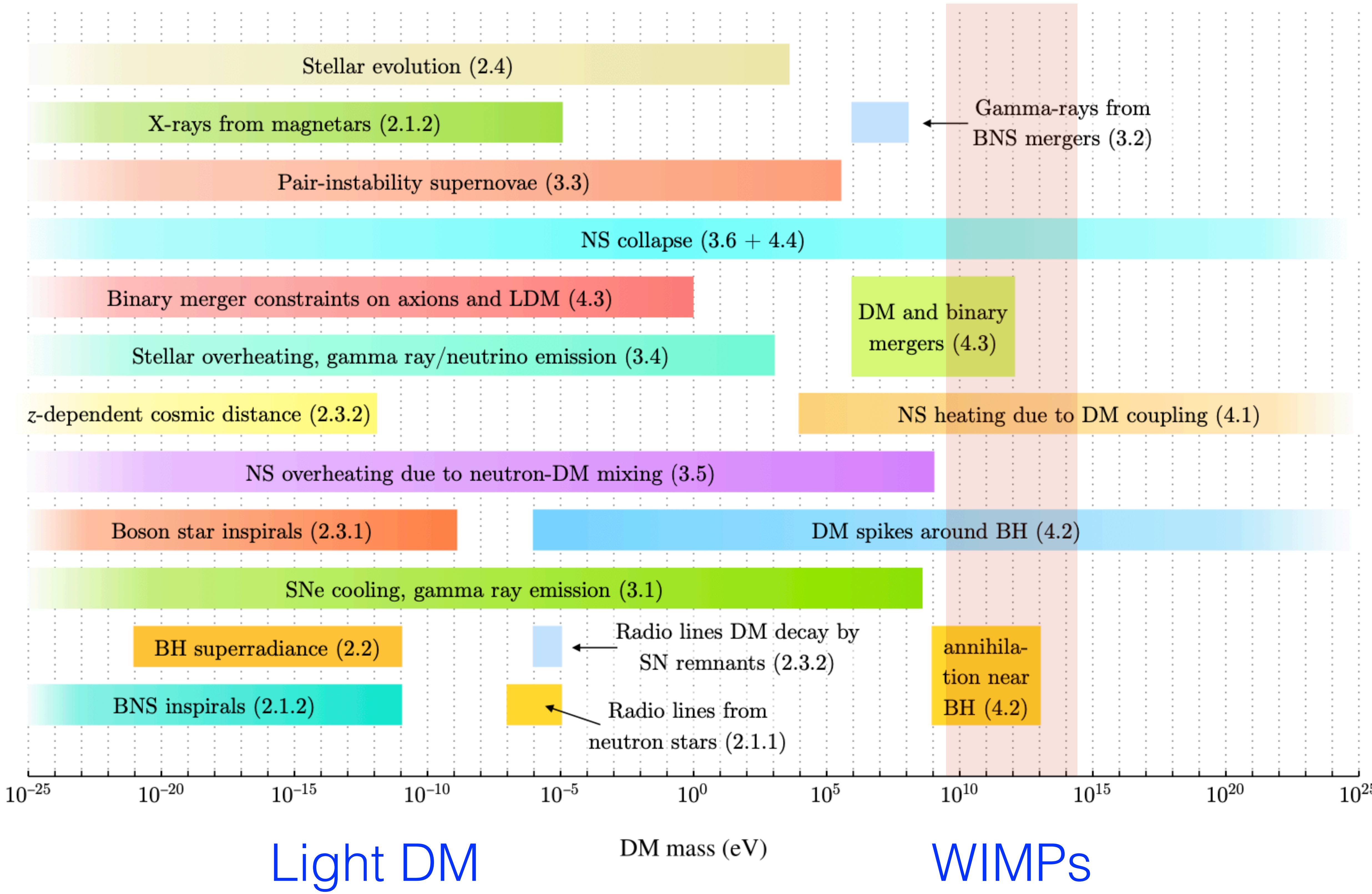

Axion Searches

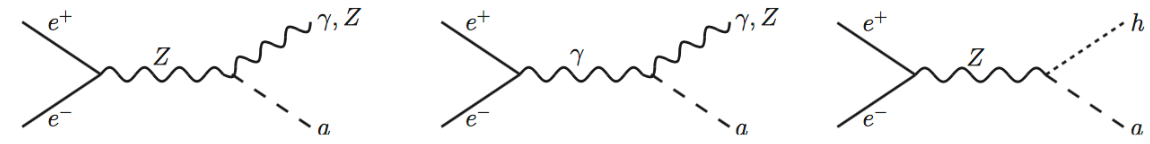

$a \to gg$

$a \to \gamma\gamma$

$a \to \ell^+\ell^-$

$Z \to \gamma a$

$$\mathcal{L}_a \sim \frac{1}{2}(\partial_\mu a)^2 - \frac{1}{2}m_a^2 a^2 + \frac{c_1}{f}\partial_\mu a \bar{f}\gamma_\mu\gamma_5 f$$
$$- \frac{c_2}{f} a G_{\mu\nu}\tilde{G}^{\mu\nu} - \frac{c_3}{f} a F_{\mu\nu}\tilde{F}^{\mu\nu} - \frac{c_4}{f} a F_{\mu\nu}\tilde{Z}^{\mu\nu} - \frac{c_5}{f} a Z_{\mu\nu}\tilde{Z}^{\mu\nu}$$
$$+ \frac{c_6}{f^2}(\partial_\mu a)(\partial^\mu a)\phi^\dagger\phi + \frac{c_7}{f^3}(\partial^\mu a)(\phi^\dagger \iota D_\mu \phi + h.c.)\phi^\dagger\phi + \ldots$$

$h \to aa$

$h \to Za$

Probe at LHC

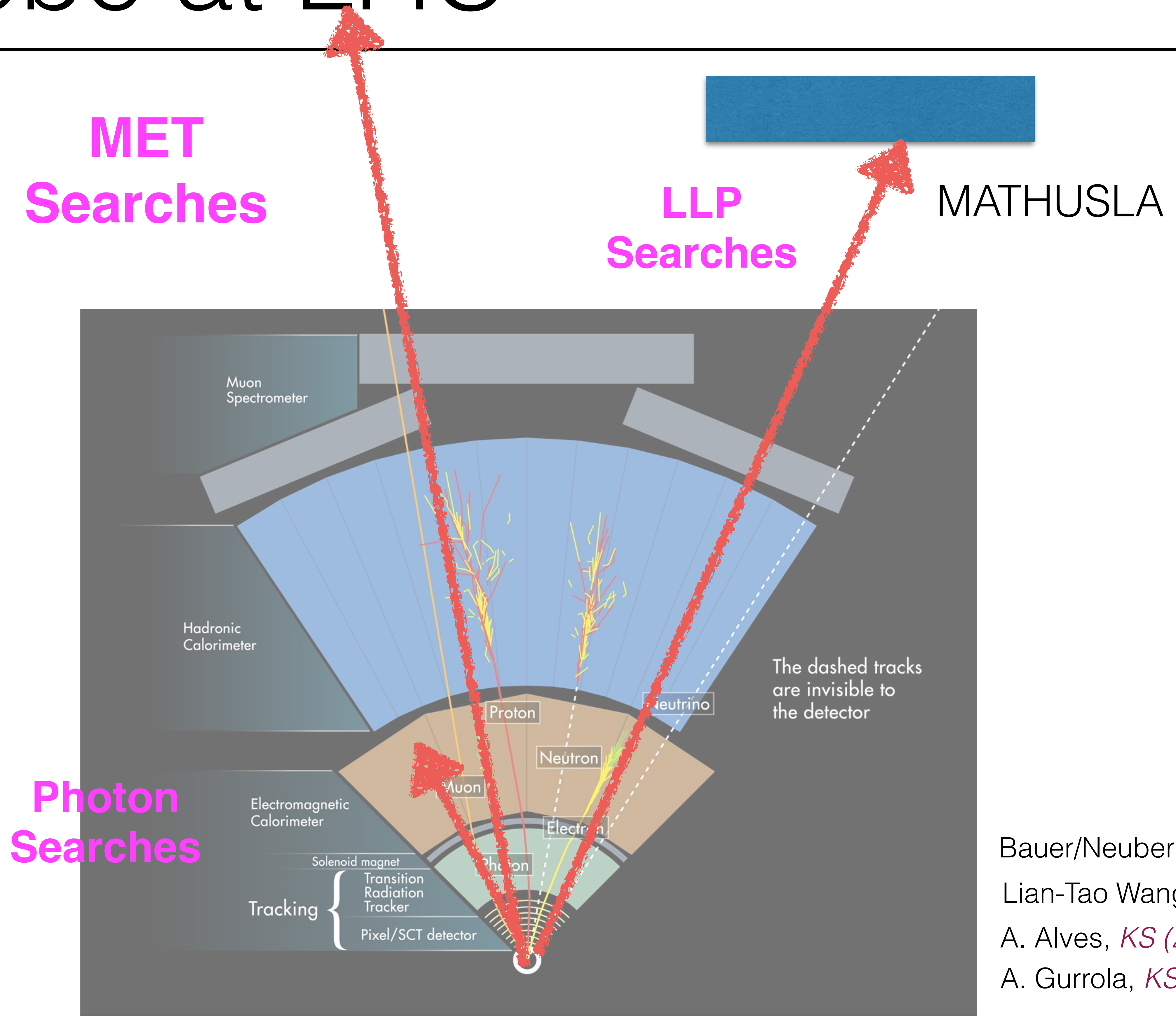

Bauer/Neubert (2018)

Lian-Tao Wang et. al. (2017)

A. Alves, *KS (2017)*

A. Gurrola, *KS (2021)*

Probe with Magnetars

Galactic Conversion Searches

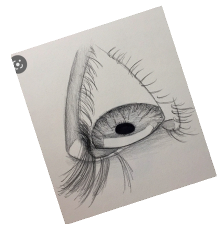

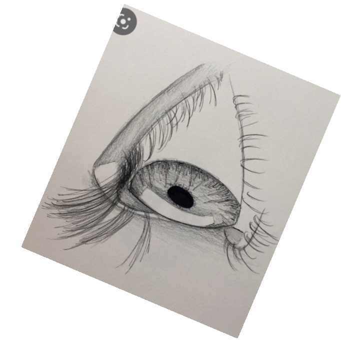

Huge literature; challenges include correctly modeling the galactic magnetic field

Galactic magnetic field

Magnetosphere Conversion Searches

$$B = B_0 (r_0/r)^3$$

$$B_0 = 20 \times 10^{14}\ \mathrm{G}$$

“Thermal” Searches

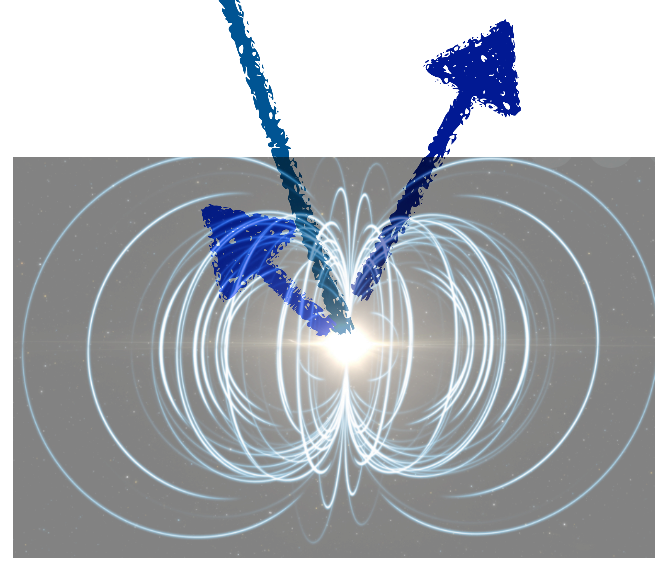

Int.J.Mod.Phys.D 30 (2021) 07

JCAP 06 (2021) 036

JCAP 11 (2019) 020

JHEP 01 (2019) 163

JHEP 06 (2018) 048

*Fortin, **KS**, Guo, Harris*

Multidisciplinary Research Teams

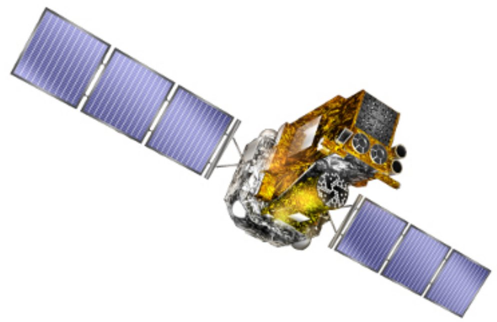

Observation

Paula Chadwick, Henric Krawczyński,

Astrophysics background modeling

Zorawar Wadiasingh
Matthew Baring

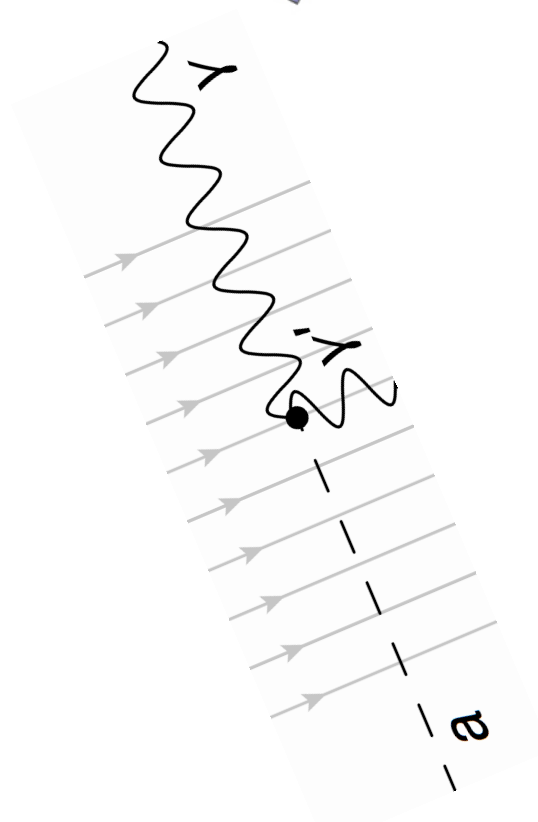

Conversion

KS, Jean-Francois Fortin

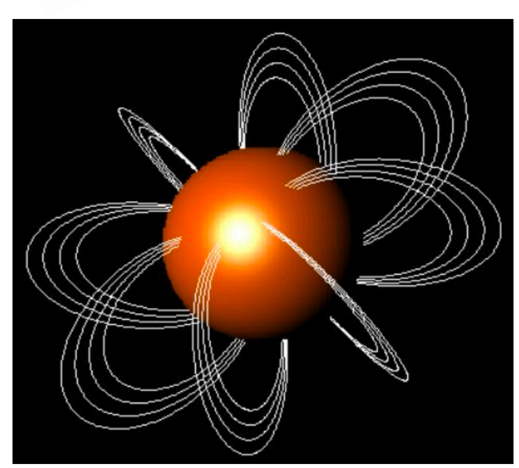

Production

Mark Alford, Steven Harris

Production

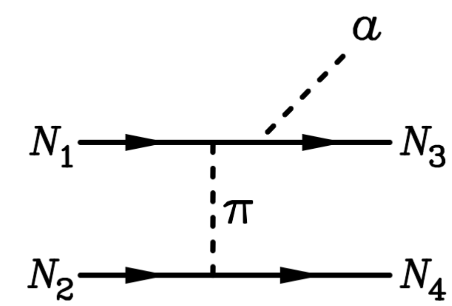

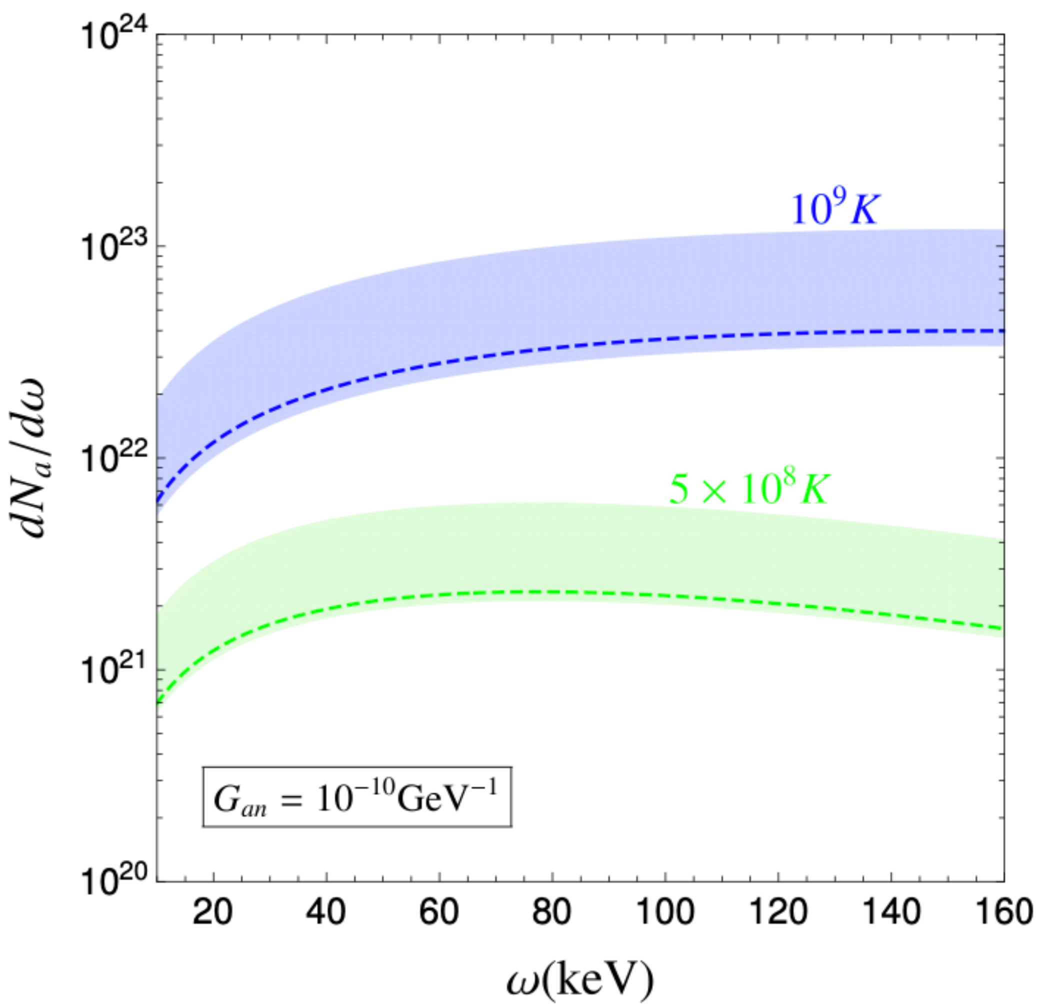

Temperature Dependence

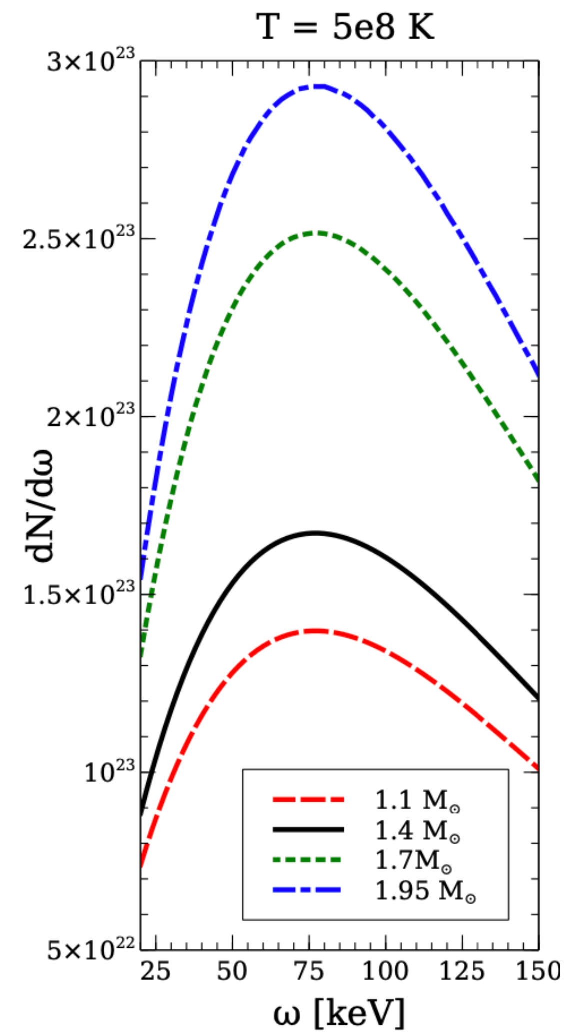

IUF EoS and with 1S0 CCDK proton superfluidity

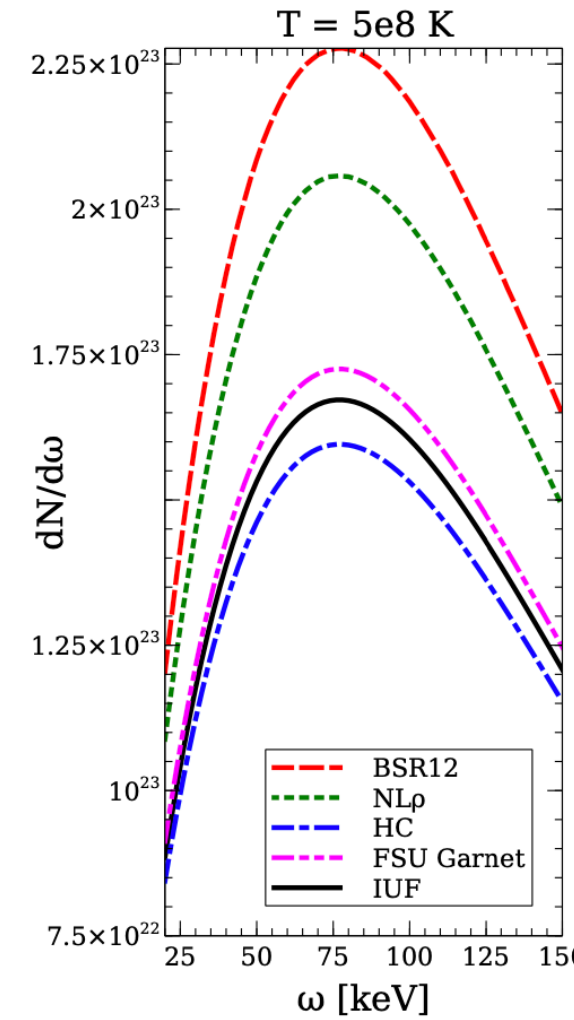

1.4M⊙ neutron star with proton 1S0 CCDK proton superfluidity,

Conversion/Propagation

Propagation equations

$$i\frac{d}{dr}\begin{pmatrix} a \\ E_{\parallel} \end{pmatrix} = \begin{pmatrix} \omega + \Delta_a & \Delta_M \\ \Delta_M & \omega + \Delta_{\parallel} \end{pmatrix}\begin{pmatrix} a \\ E_{\parallel} \end{pmatrix}$$

Raffelt/Stodolsky (1988)

Semi-analytic conversion probability

$$P_{a\to\gamma} = \left(\frac{\Delta_{M0} r_0^3}{r_{a\to\gamma}^2}\right)^2 \times \begin{cases} \frac{\pi}{3|\Delta_a r_{a\to\gamma}|} e^{\frac{6\Delta_a r_{a\to\gamma}}{5}} & |\Delta_a r_{a\to\gamma}| \gtrsim 0.45 \\ \frac{\Gamma\left(\frac{2}{5}\right)^2}{5^{\frac{6}{5}} |\Delta_a r_{a\to\gamma}|^{\frac{4}{5}}} & |\Delta_a r_{a\to\gamma}| \lesssim 0.45 \end{cases}.$$

KS, Fortin (2018)

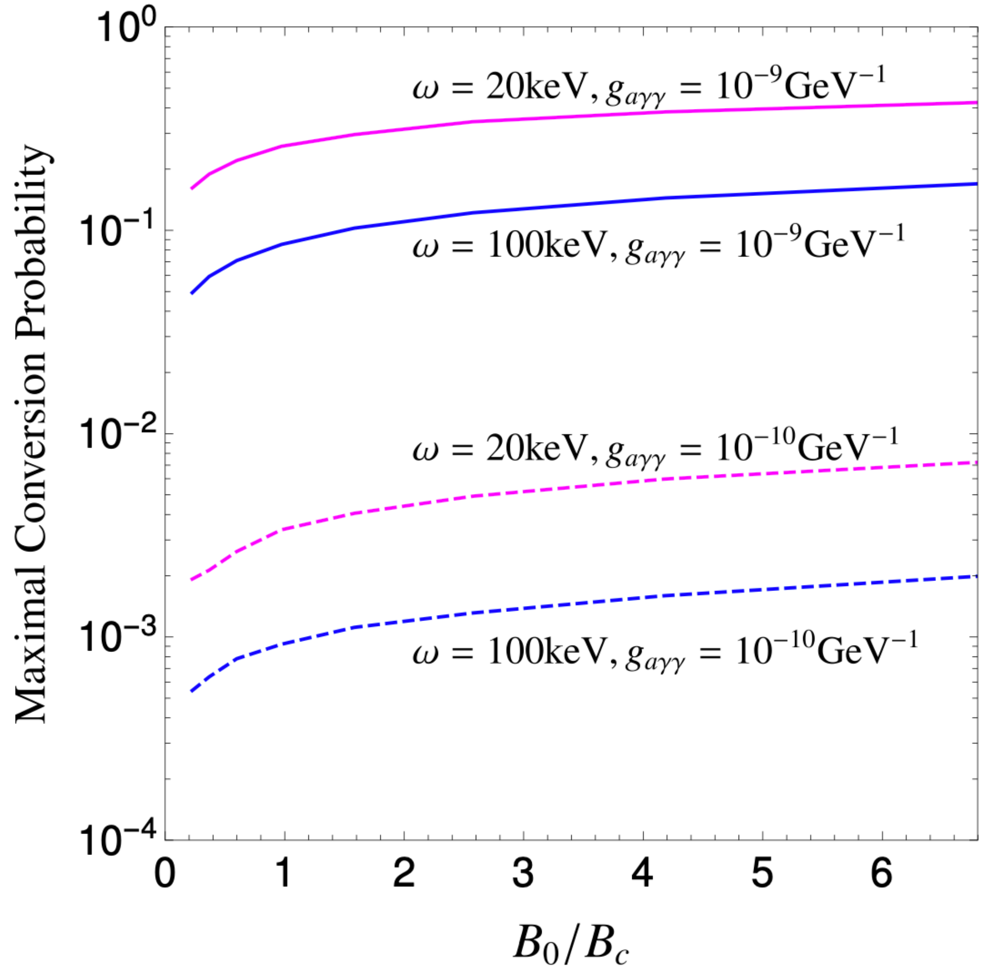

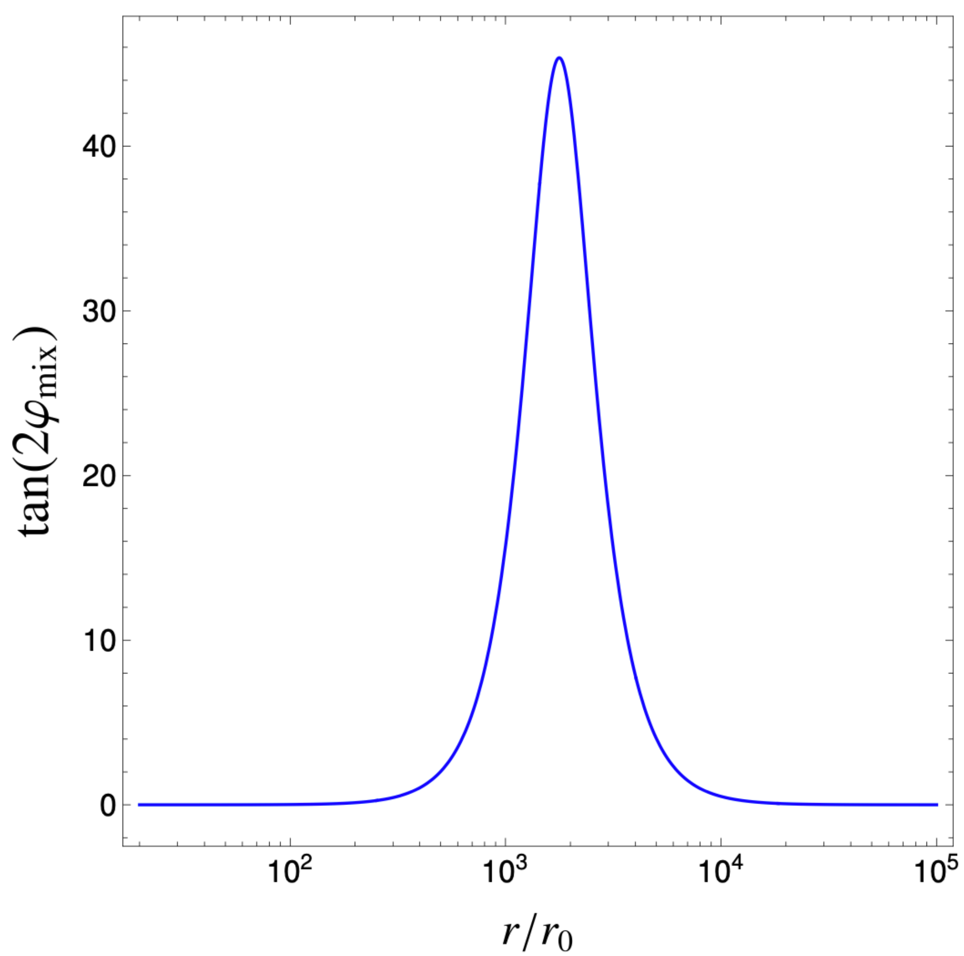

Detection

$$L_{a\to\gamma} = \int_0^\infty d\omega \frac{1}{2\pi}\int_0^{2\pi} d\theta \cdot \omega \cdot \frac{dN_a}{d\omega} \cdot P_{a\to\gamma}(\omega,\theta).$$

$$\nu F_\nu(\omega) = \omega^2 \frac{1}{4\pi D^2}\frac{1}{\omega}\frac{dL_{a\to\gamma}}{d\omega}.$$

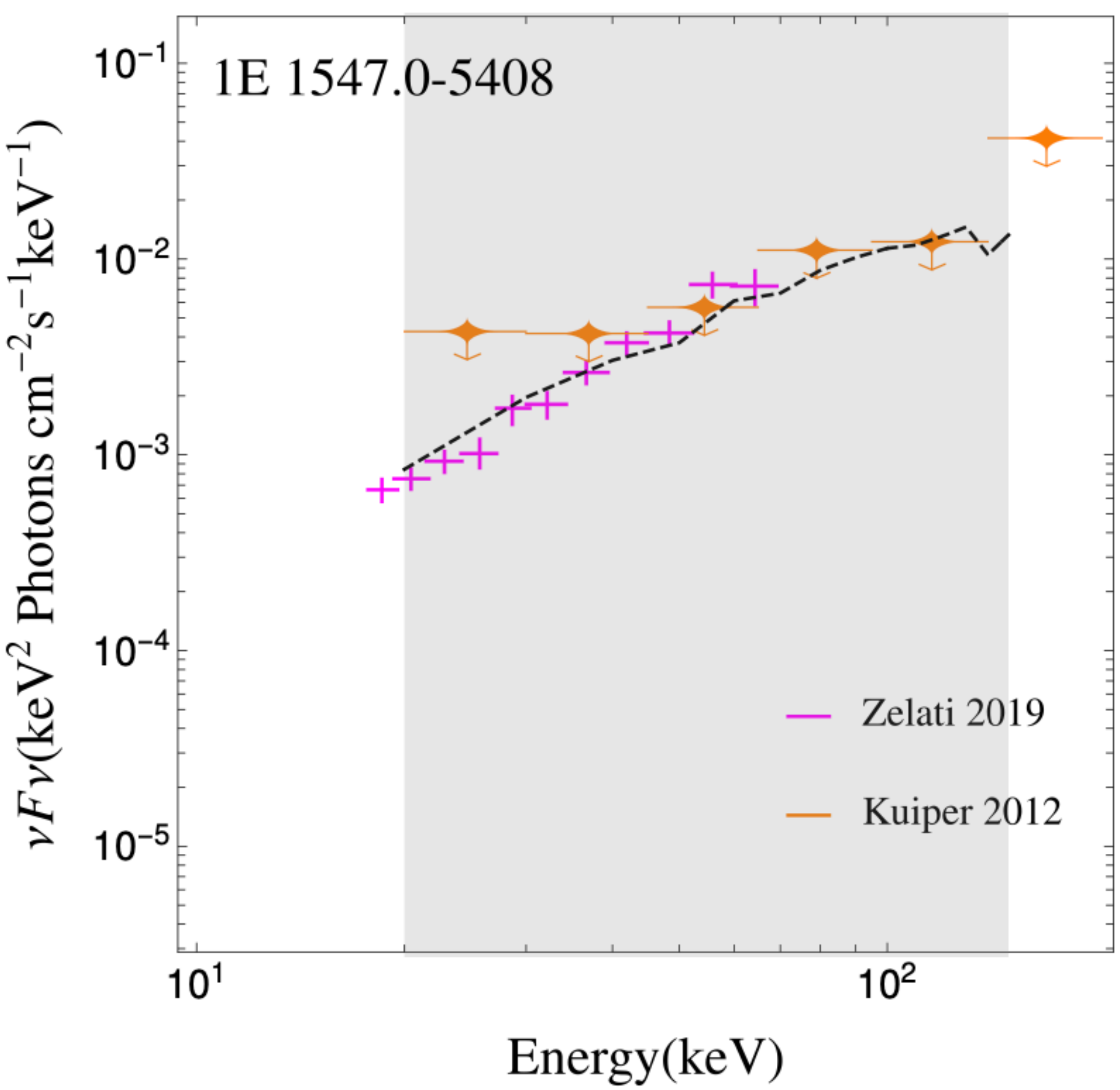

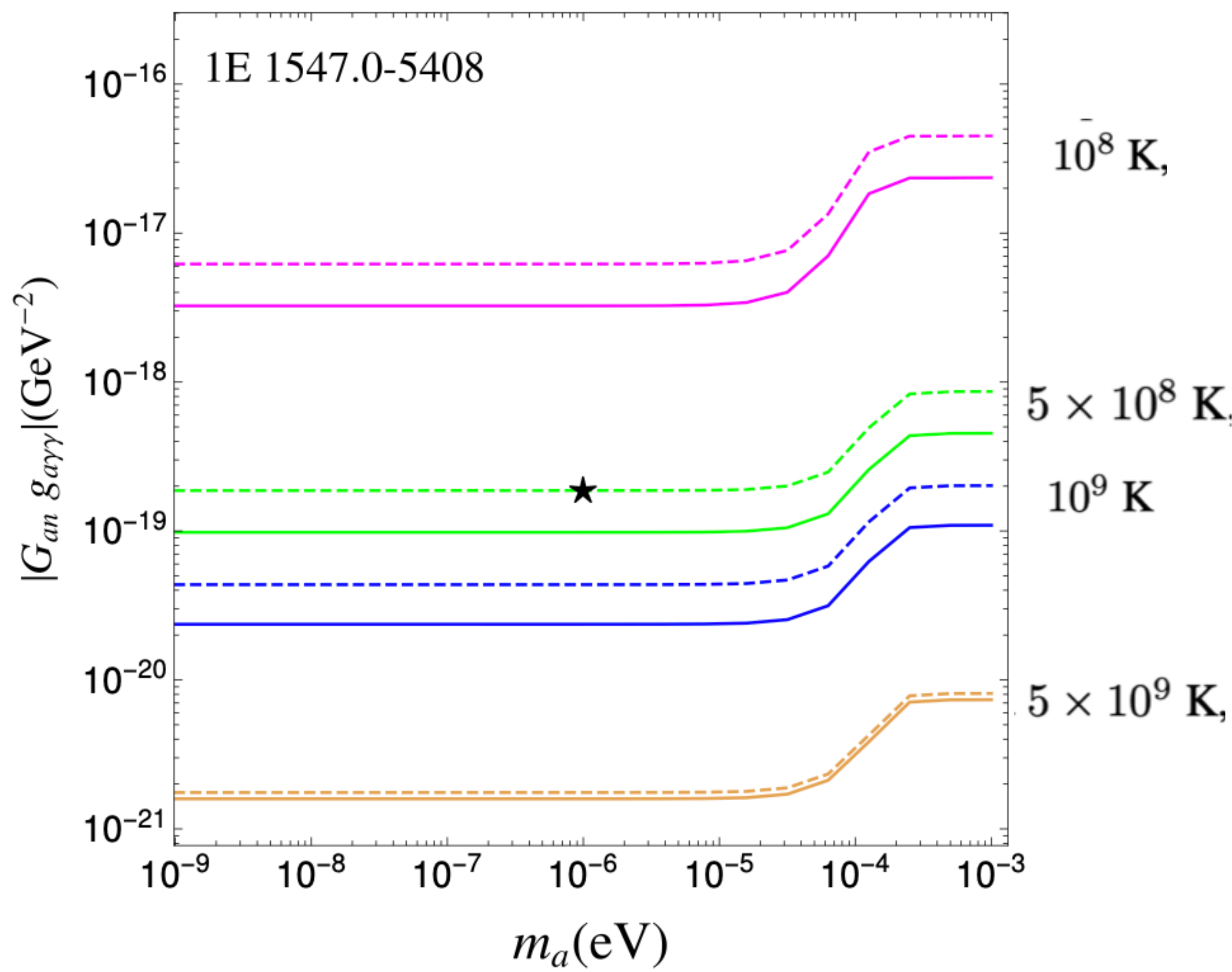

NuSTAR (magenta), INTEGRAL (orange)

Prospects

Hot magnetars with high
magnetic fields close to Earth are the best

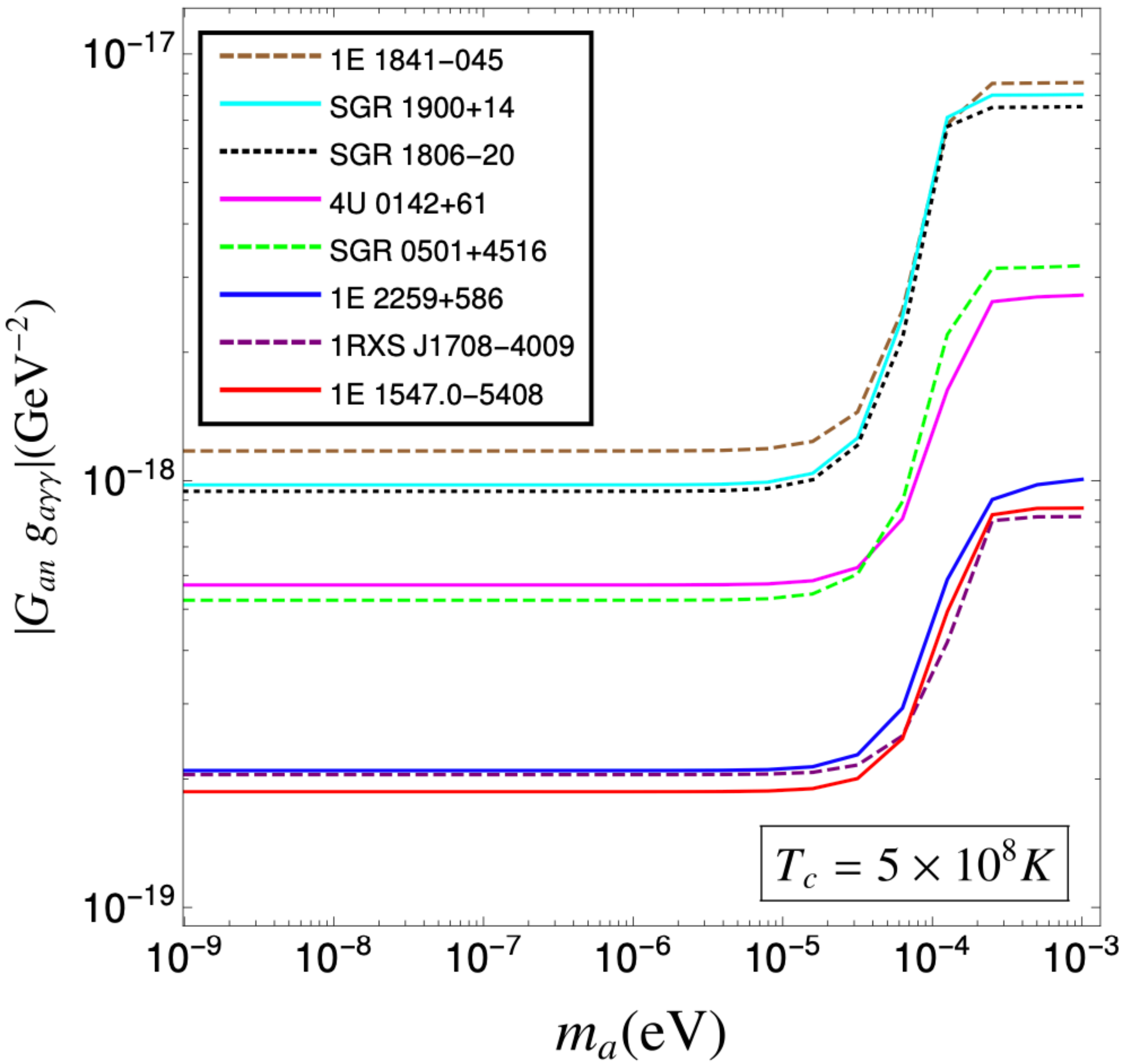

Name	B ($10^{14} G$)	D (kpc)
SGR 1806-20	7.7	8.7
1E 1547.0-5408	6.4	4.5
4U 0142+61	1.3	3.6
SGR 0501+4516	1.9	3.3
1RXS J170849.0-400910	4.7	3.8
1E 1841-045	7	8.5
SGR 1900+14	7	12.5
1E 2259+586	0.59	3.2

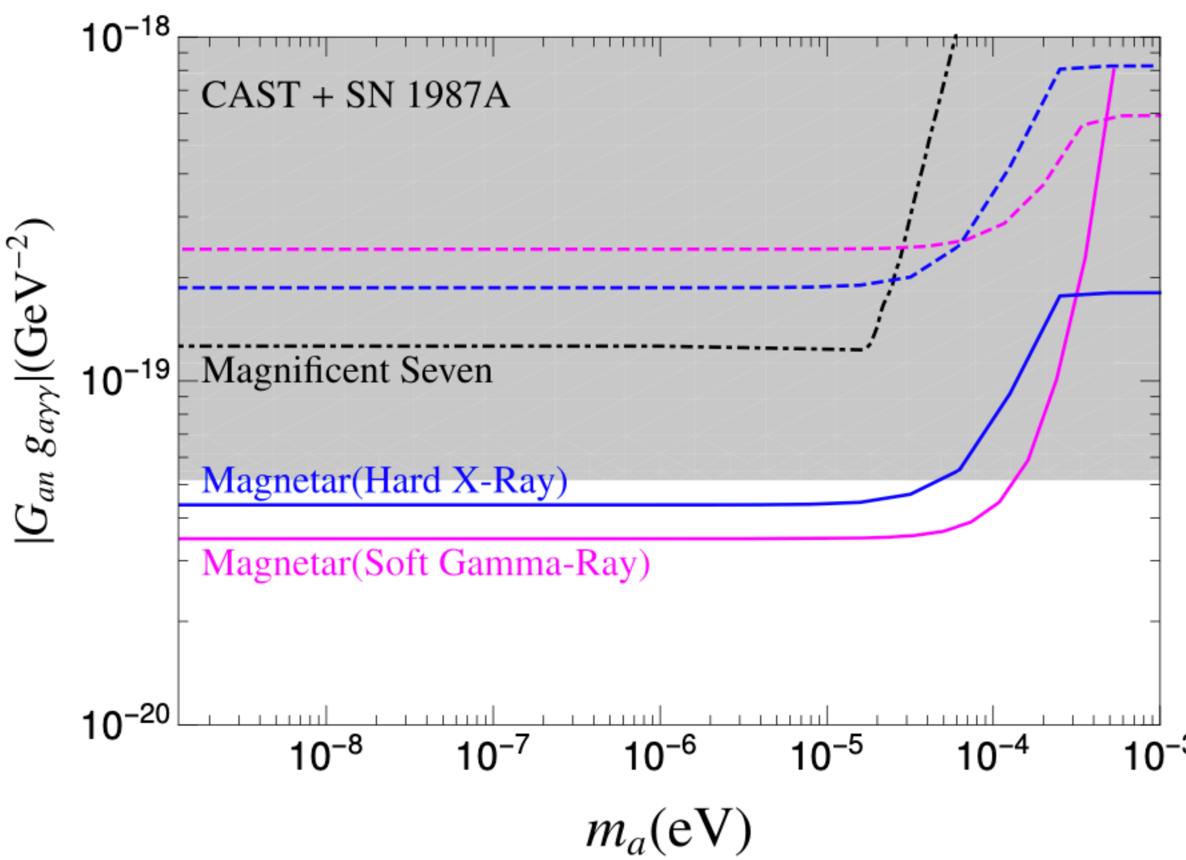

Polarization

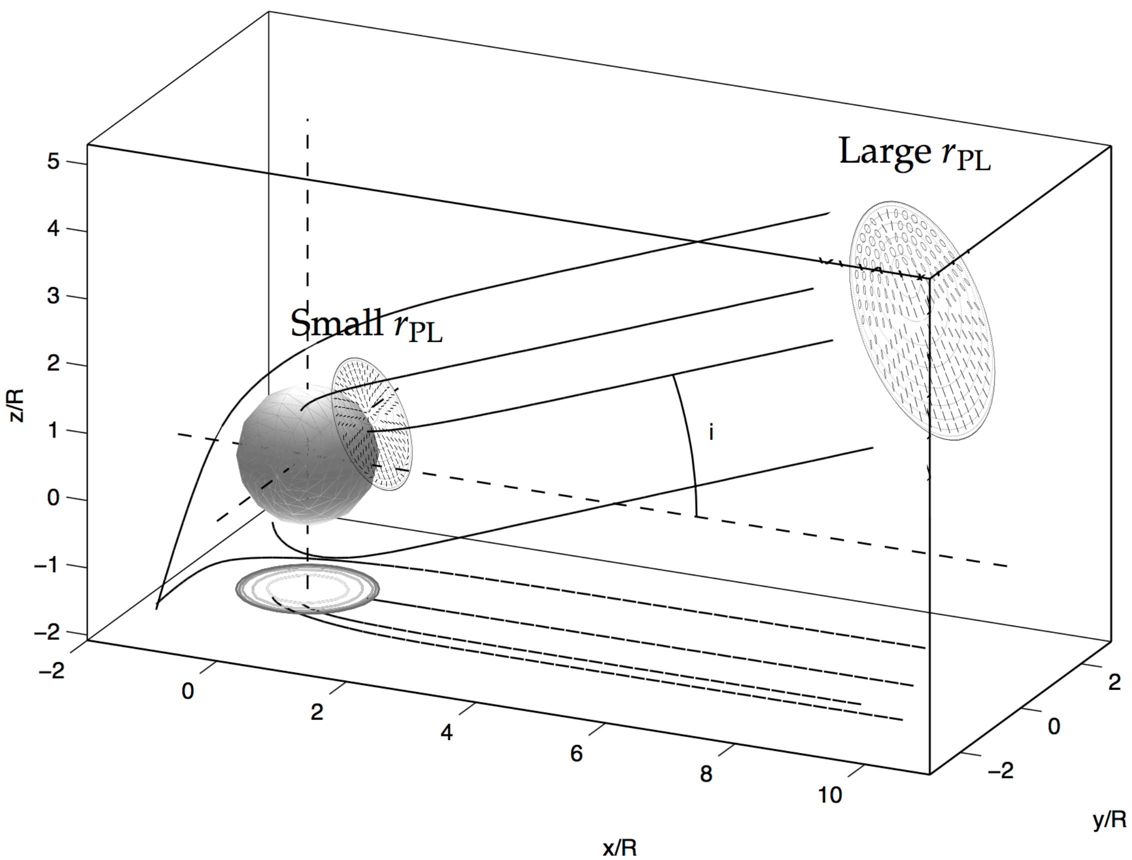

Krawczynski, KS, Fortin (in progress)

$r_{a \to \gamma}$

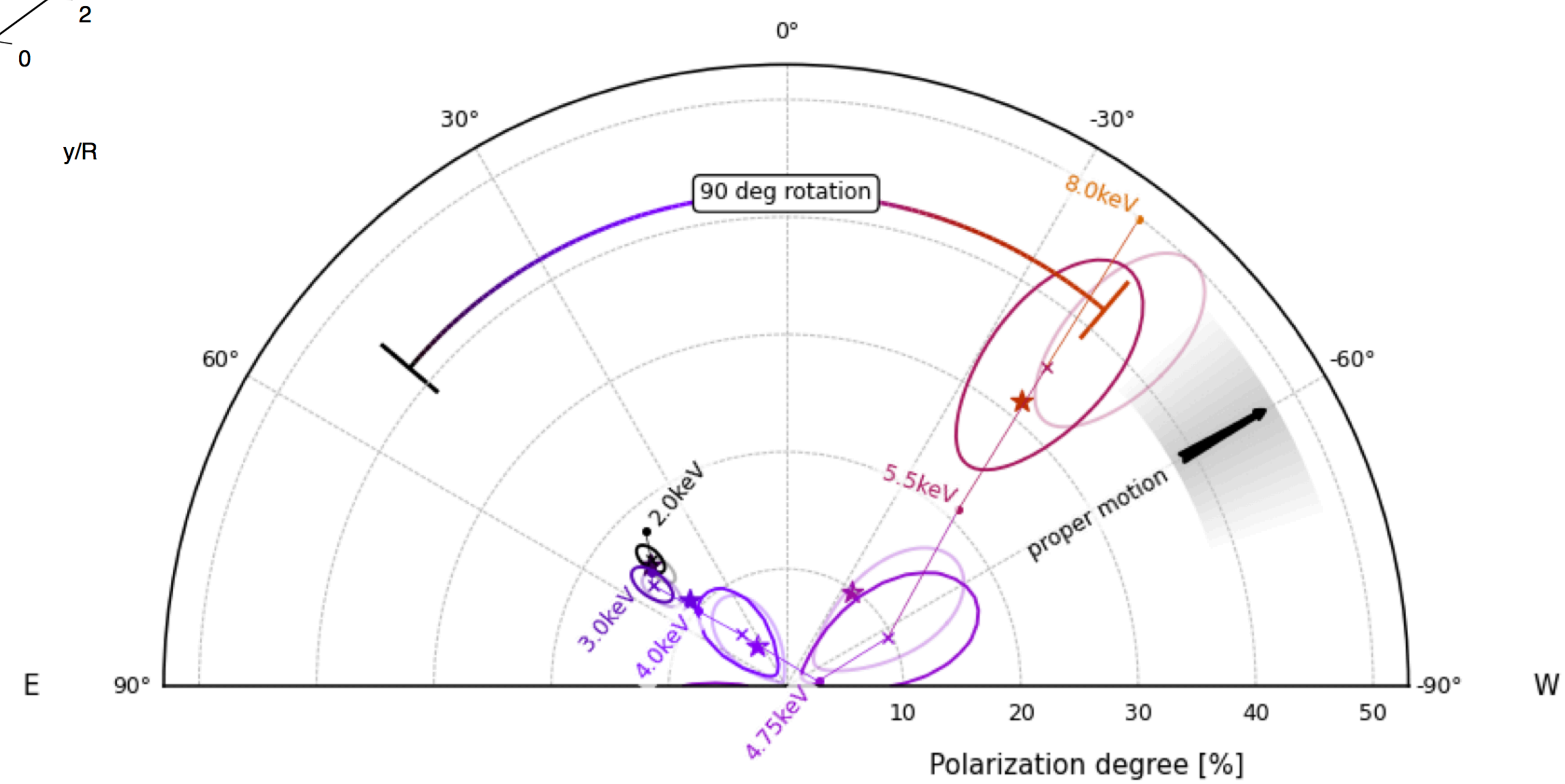

IXPE observation of 4U 0142+61

Probe with NS Mergers

Galactic Conversion Searches

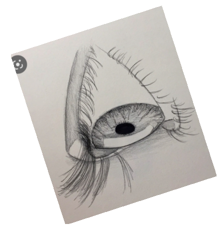

Fabio Iocco (2023)

Fermi-LAT

Galactic magnetic field

$a \to \gamma\gamma$

Decay Searches

Clough, Dietrich

“Thermal” Searches

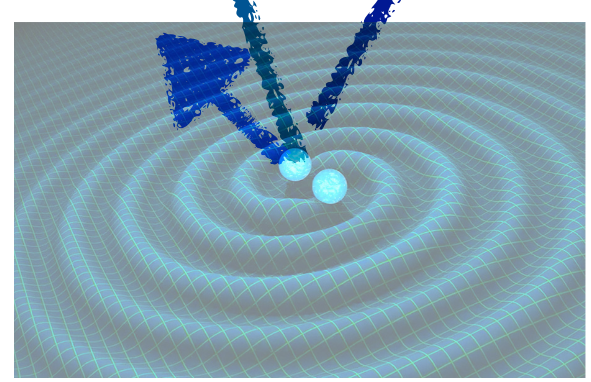

Can cooling change the GW signal?

Trapping affects the shear viscosity, thermal conductivity, etc.

Difficult problem

Probe with NS Mergers

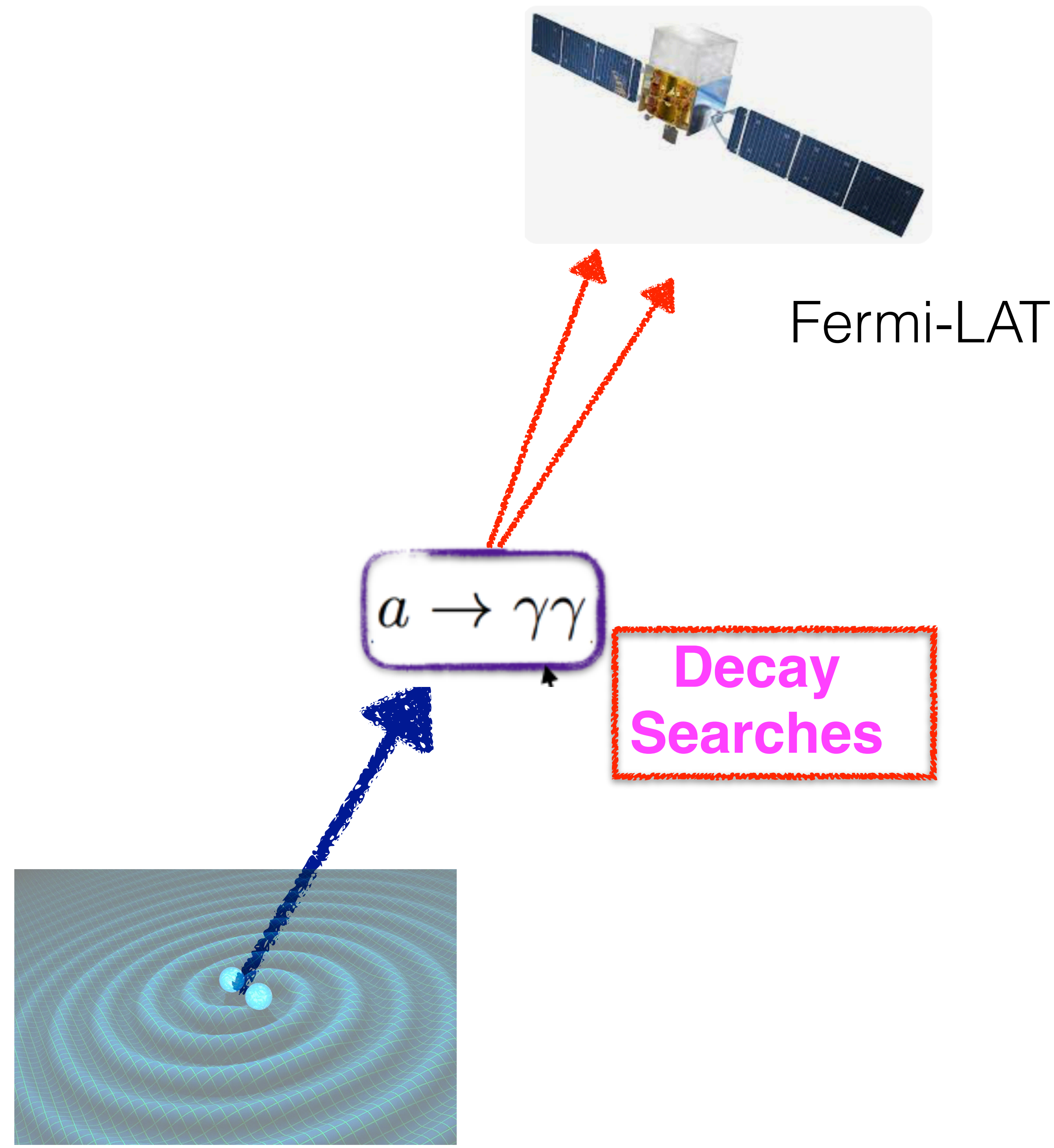

Production: Primakoff and Photon Fusion

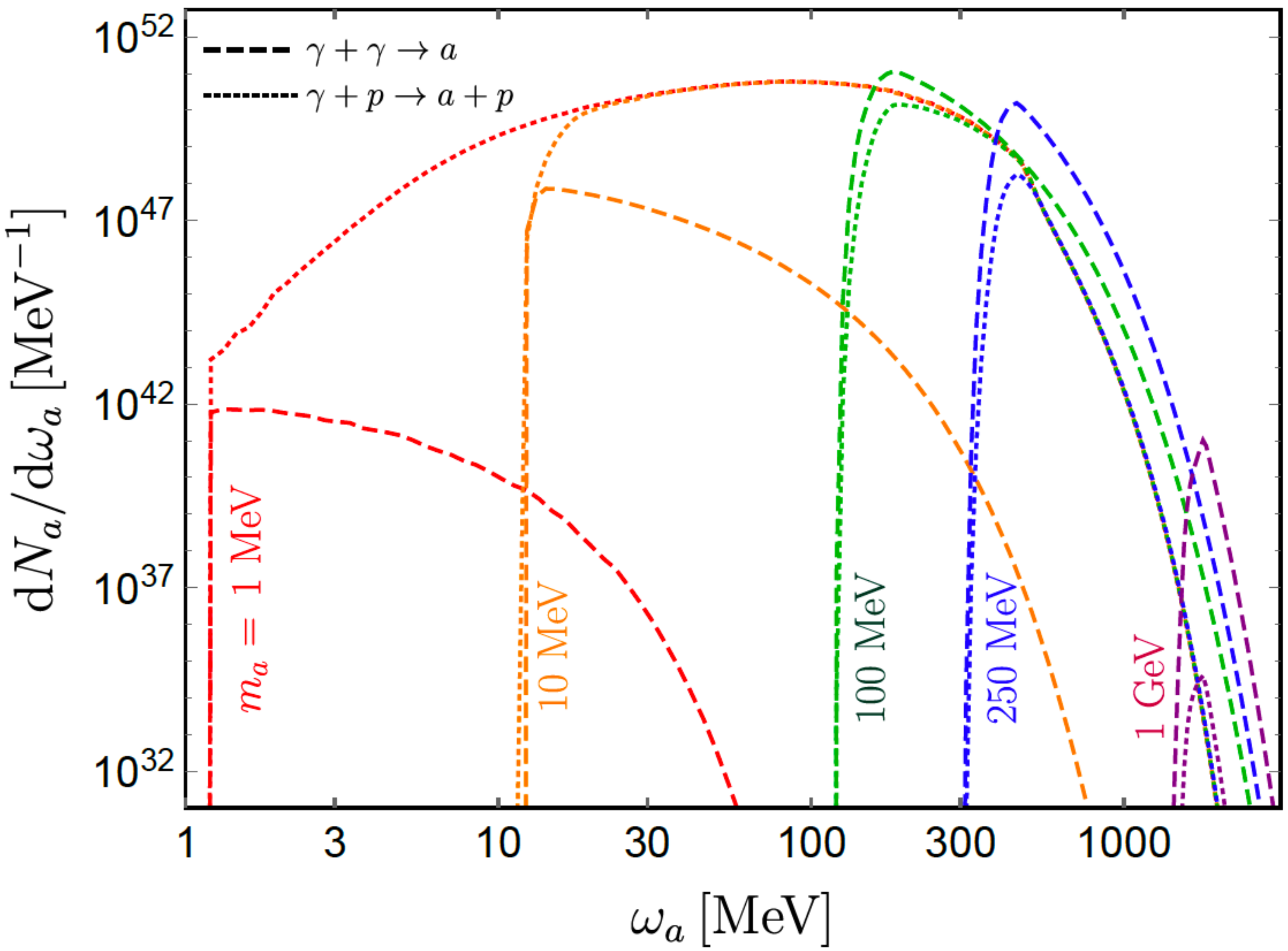

FIG. 2. ALP production spectrum from a merger remnant, assuming constant emission over the course of one second. The ALP-photon coupling is set to $g_{a\gamma\gamma} = 10^{-10}\,\text{GeV}^{-1}$. Note the switchover between Primakoff and photon coalescence at $m_a \approx 100\,\text{MeV}$.

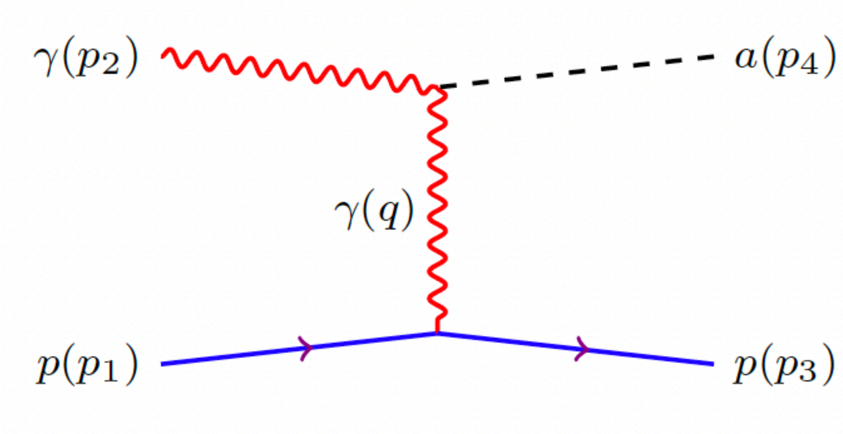

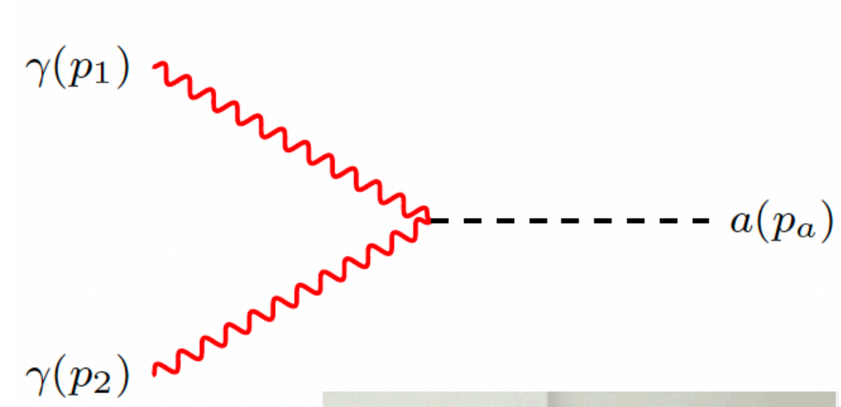

Steven Harris, U. Wash

Production: Gravitational Trapping Effects

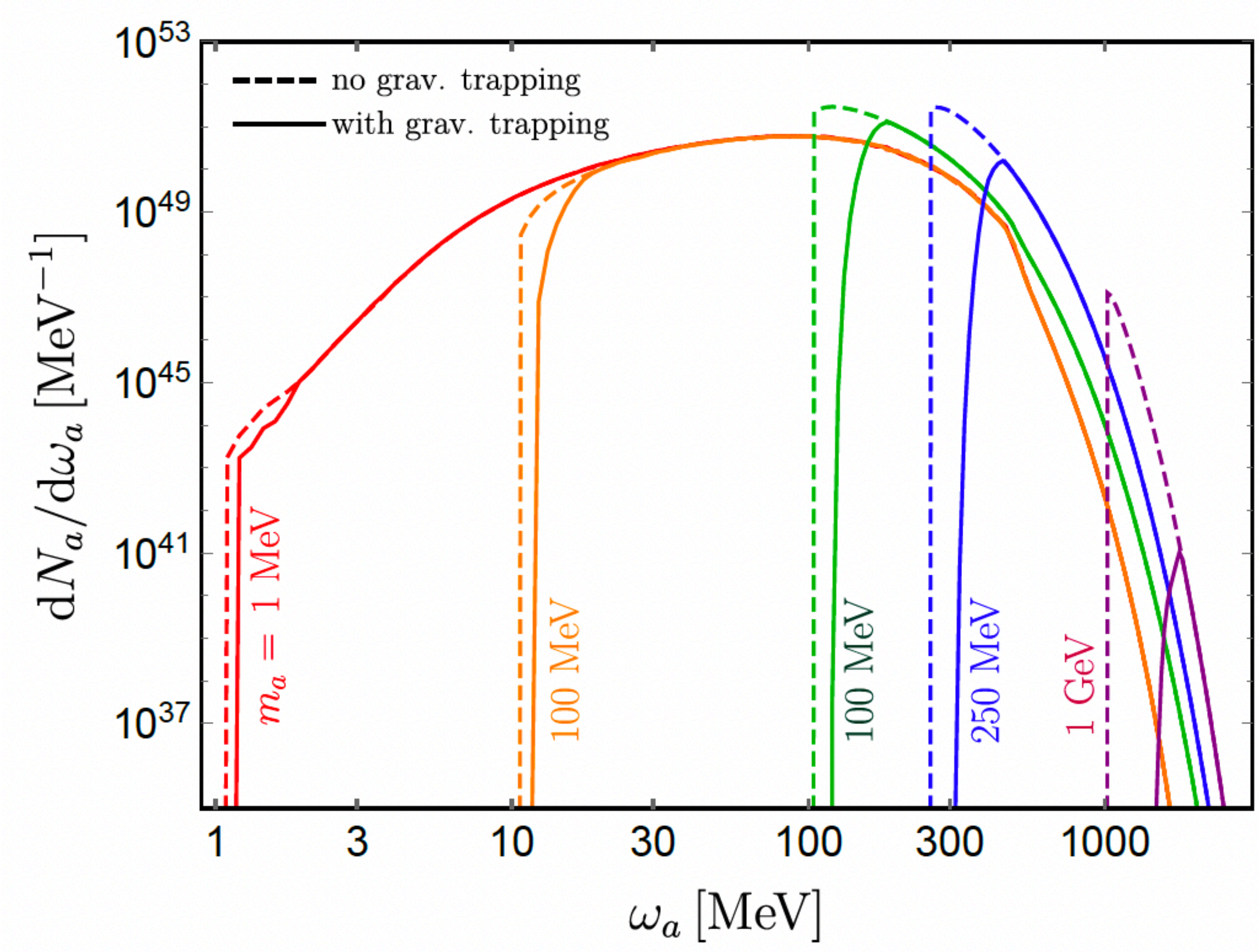

The spectrum 'starts up" only for ALP energies $E_a \gtrsim 1.5 - 1.7 m_a$.

supernova counterpart, Fig. 11 in Ref. [72], where the spectrum starts up at $E_a \gtrsim 1.12 m_a$.

to its supernova counterpart, Fig. 11 in Ref. [72], where the spectrum starts up at $E_a \gtrsim 1.12 m_a$. The supernova evidently has less significant gravitational trapping because the dense core of the supernova where most of the ALPs are produced is less compact than a NS merger remnant (cf. Fig. S2).

NS Merger Profiles

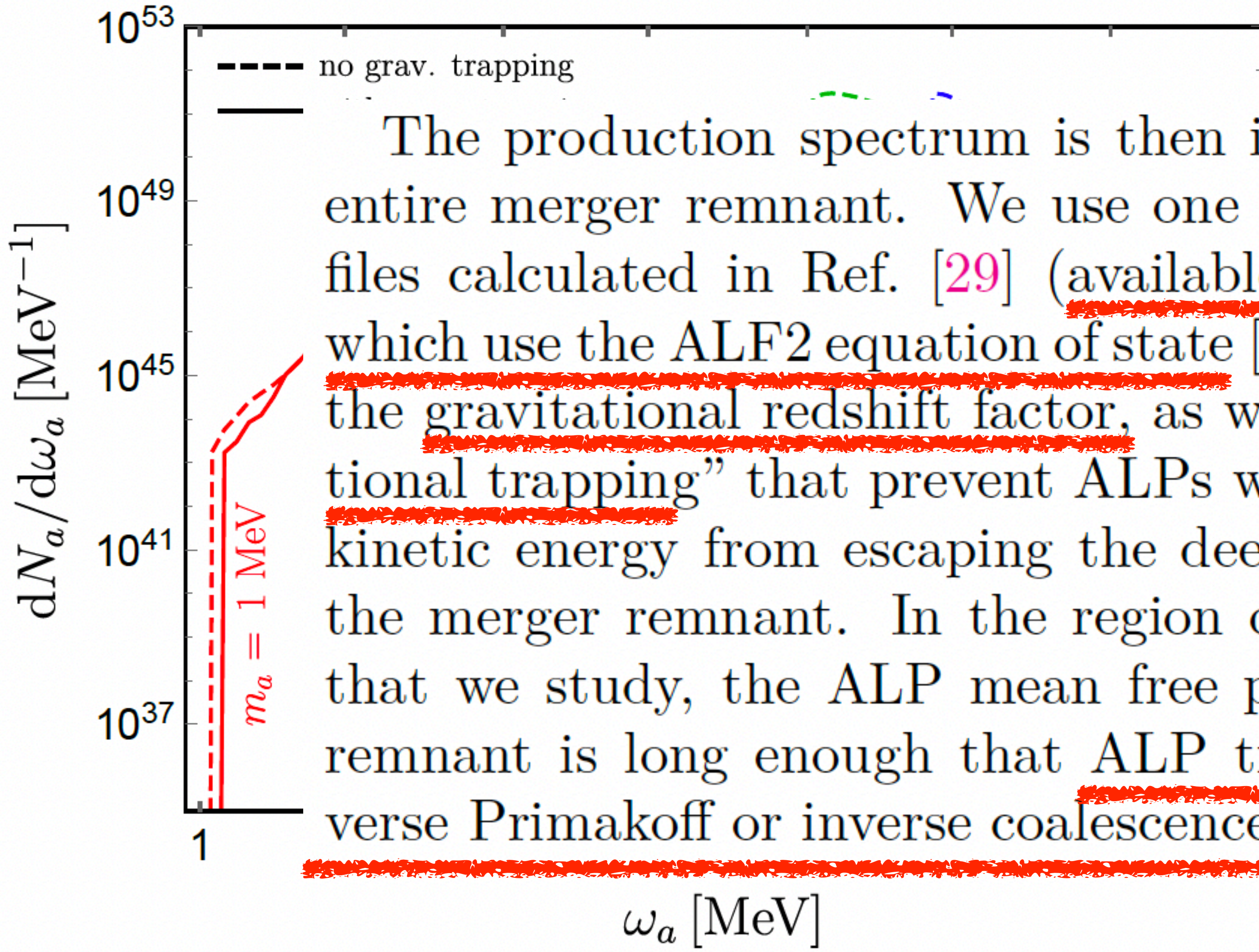

The production spectrum is then integrated over the entire merger remnant. We use one of the merger profiles calculated in Ref. [29] (available on `Zenodo` [30]), which use the ALF2 equation of state [31, 32]. We include the gravitational redshift factor, as well as the "gravitational trapping" that prevent ALPs with sufficiently low kinetic energy from escaping the deep potential well of the merger remnant. In the region of parameter space that we study, the ALP mean free path in the merger remnant is long enough that ALP trapping due to inverse Primakoff or inverse coalescence is negligible.

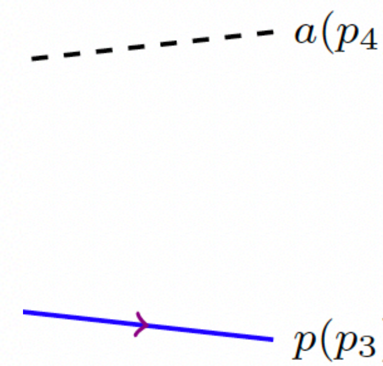

NS Merger Profiles

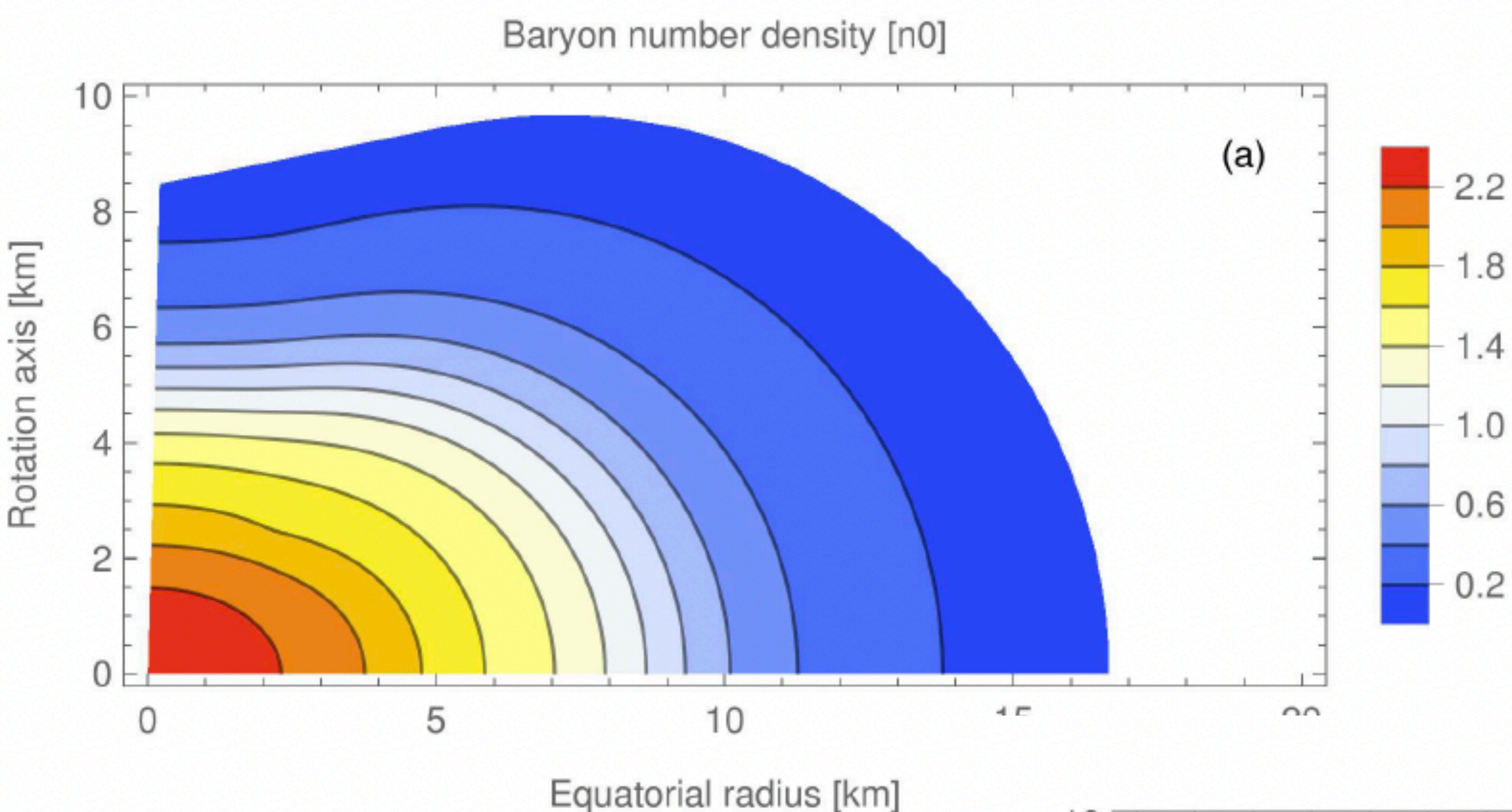

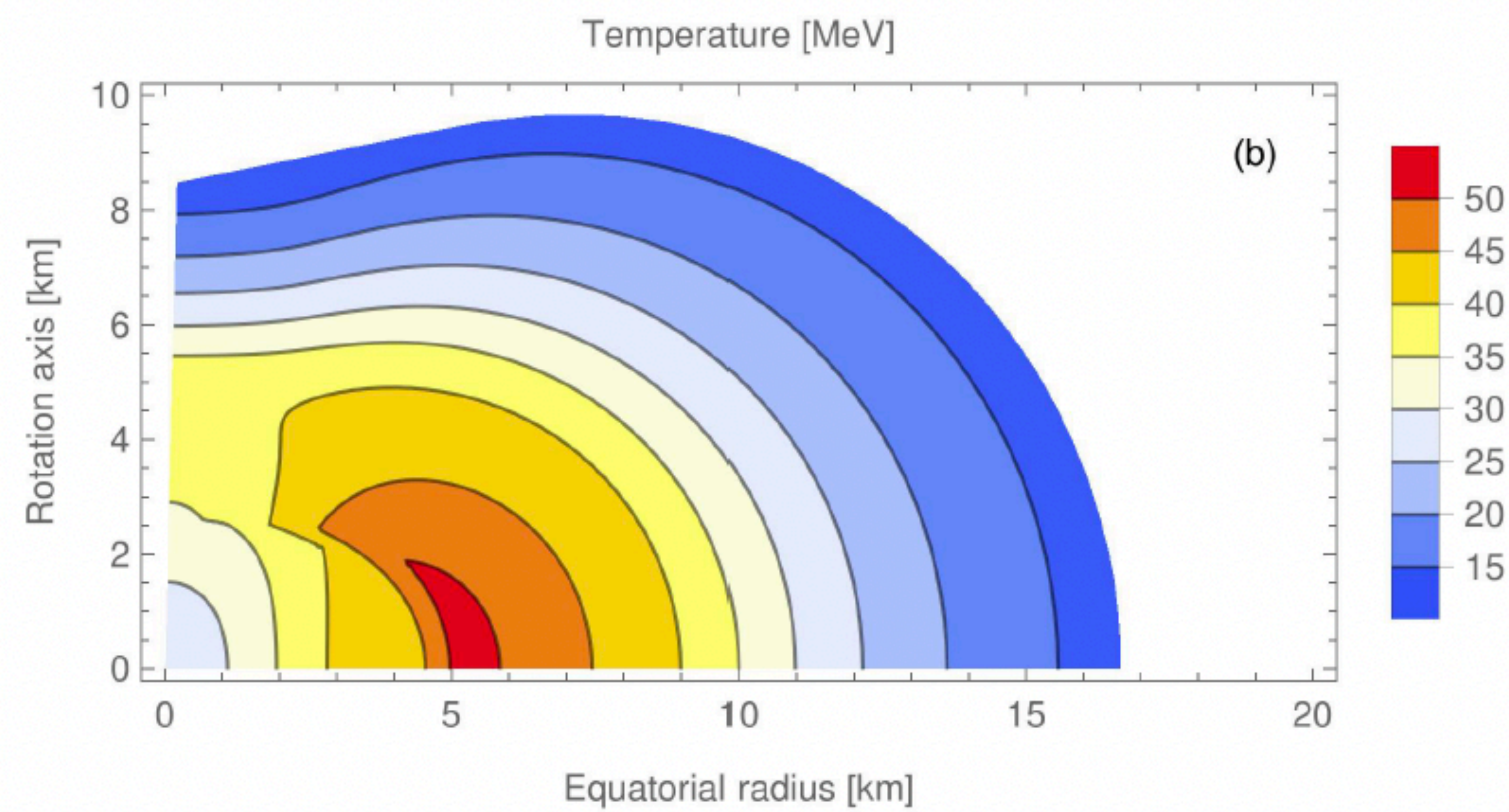

NS Merger Profiles

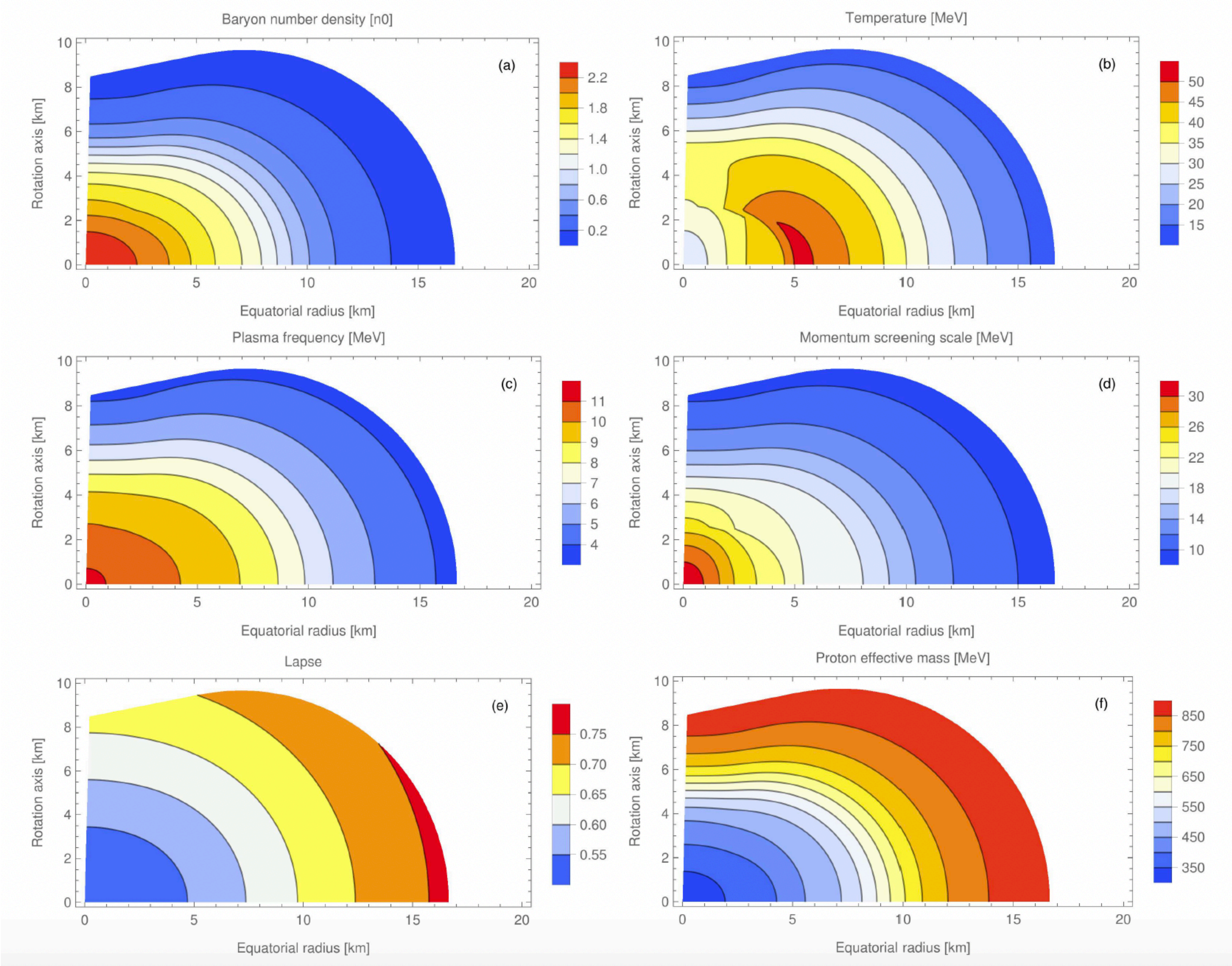

Production for Different Profiles

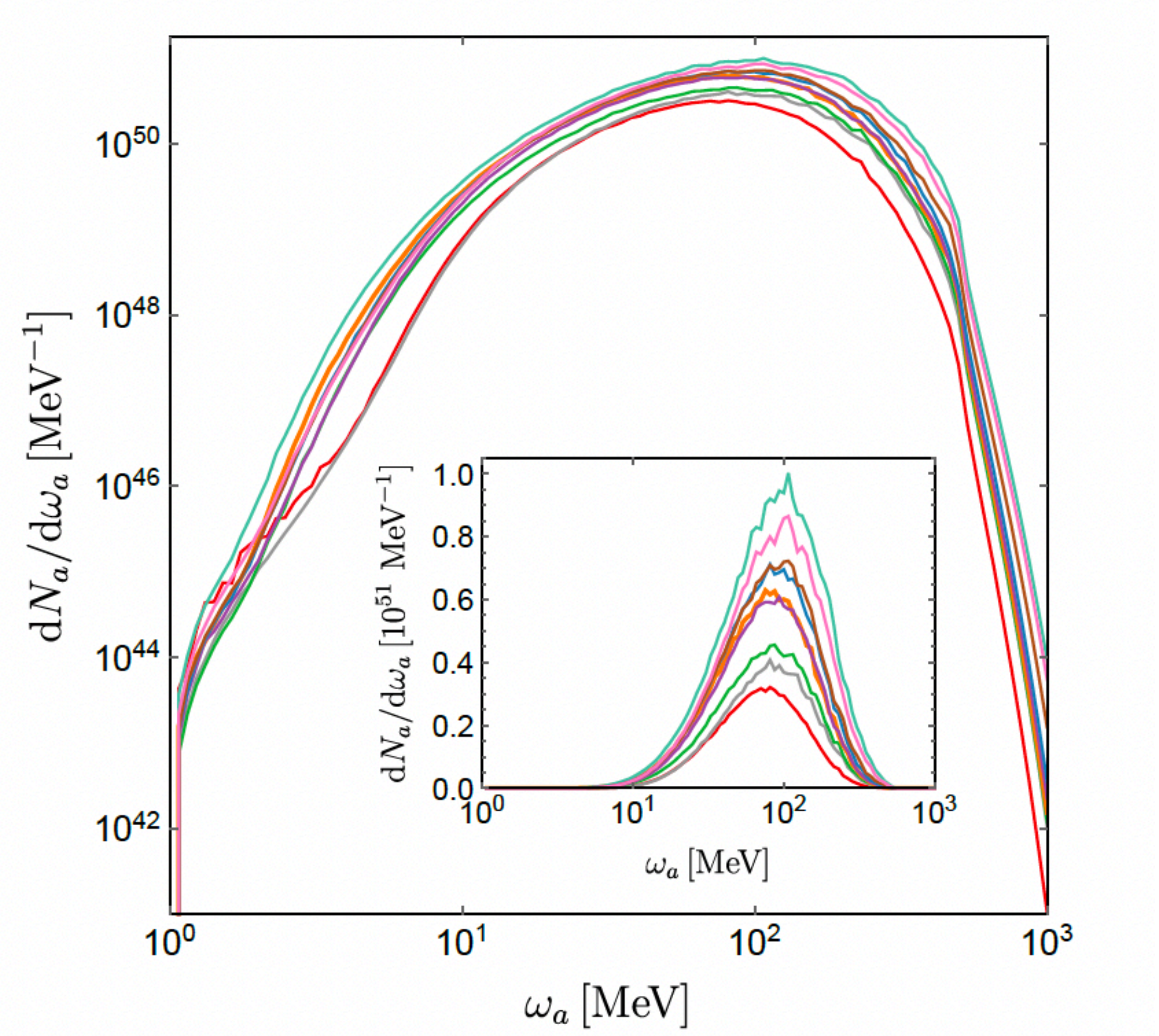

FIG. S3. ALP production spectra for nine merger profiles presented in Ref. [29], for an ALP with $m_a = 1$ MeV, $g_{a\gamma\gamma} = 10^{-10}$ GeV^{-1} and an ALP emission duration of 1 sec. The bold, orange curve represents the profile we consider in our analysis in the

Decay

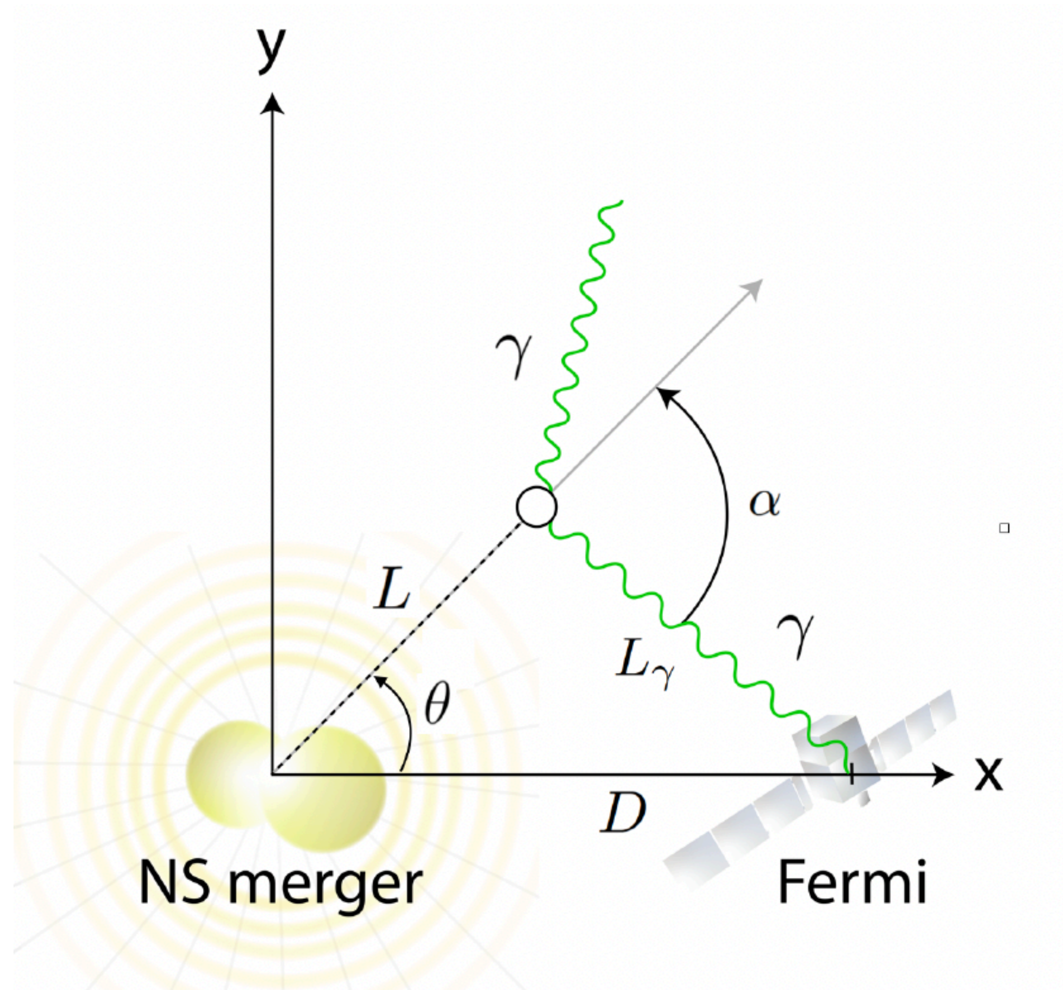

$$\omega_\gamma^2 \frac{\mathrm{d}^2 F_\gamma}{\mathrm{d}\omega_\gamma \mathrm{d}t}(\omega_\gamma, D+t) = \int_{-1}^{1} \mathrm{d}z \int_0^\infty \mathrm{d}L \, \frac{\omega_\gamma^2}{4\pi D(L_\gamma + Lz)} \frac{\mathrm{d}^2 N_a}{\mathrm{d}\omega_a \mathrm{d}t}(\omega_a, D+t-L/\beta_a - L_\gamma).\mathrm{Jac}(\omega_a, \omega_\gamma)$$
$$\times \frac{m_a^2}{\omega_a^2(1-\beta_a z)^2} \frac{\exp\left(-L/\ell_a\right)}{\ell_a} \Theta(L-R_\star)\Theta(L-D/\sqrt{1-z^2}) \, .$$

Spectral/Temporal Behavior

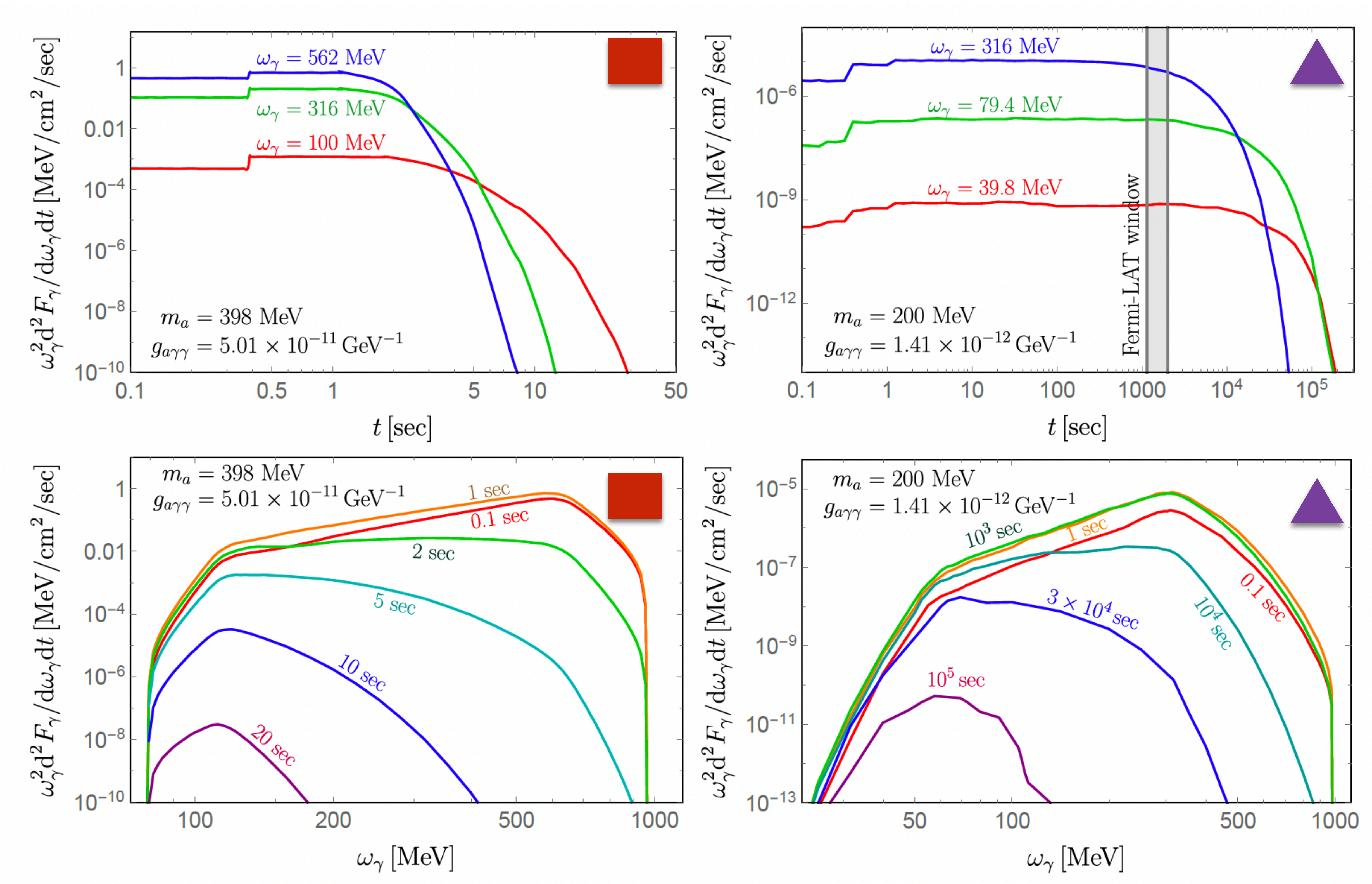

Multimessenger

Abbott et. al. (2017)

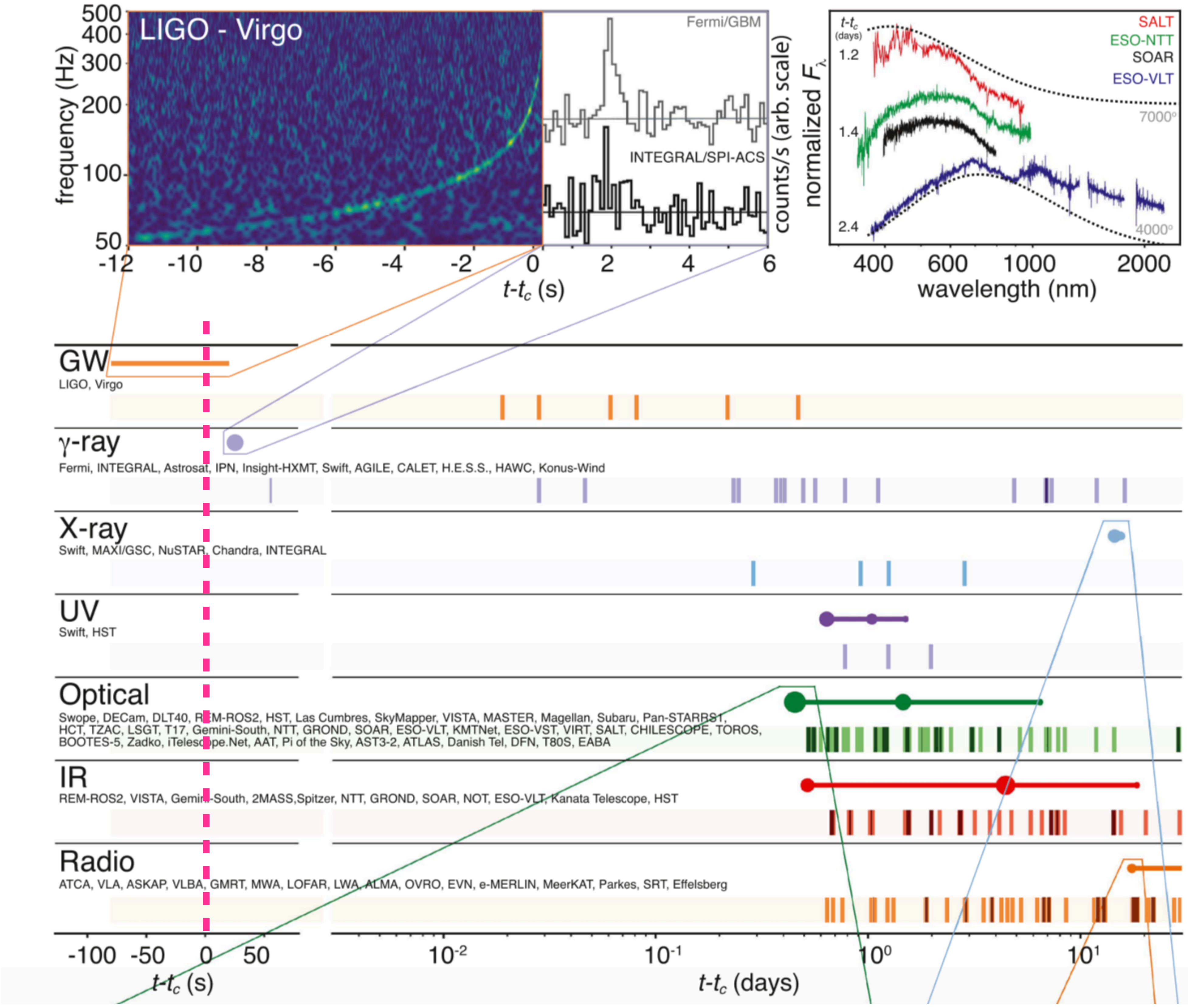

Multimessenger

Abbott et. al. (2017)

Table 3
Gamma-Ray Monitoring and Evolution of GW170817

Observatory	UT Date	Time since GW Trigger	90% Flux Upper Limit (erg cm^{-2} s^{-1})	Energy Band
Insight-HXMT/HE	Aug 17 12:34:24 UTC	−400 s	3.7×10^{-7}	0.2–5 MeV
CALET CGBM	Aug 17 12:41:04 UTC	0.0	1.3×10^{-7}[a]	10–1000 keV
Konus-*Wind*	Aug 17 12:41:04.446 UTC	0.0	3.0×10^{-7} [erg cm^{-2}]	10 keV–10 MeV
Insight-HXMT/HE	Aug 17 12:41:04.446 UTC	0.0	3.7×10^{-7}	0.2–5 MeV
Insight-HXMT/HE	Aug 17 12:41:06.30 UTC	1.85 s	6.6×10^{-7}	0.2–5 MeV
Insight-HXMT/HE	Aug 17 12:46:04 UTC	300 s	1.5×10^{-7}	0.2–5 MeV
AGILE-GRID	Aug 17 12:56:41 UTC	0.011 days	3.9×10^{-9}	0.03–3 GeV
Fermi-LAT	Aug 17 13:00:14 UTC	0.013 days	4.0×10^{-10}	0.1–1 GeV
H.E.S.S.	Aug 17 17:59 UTC	0.22 days	3.9×10^{-12}	0.28–2.31 TeV
HAWC	Aug 17 20:53:14—Aug 17 22:55:00 UTC	0.342 days + 0.425 days	1.7×10^{-10}	4–100 TeV
Fermi-GBM	Aug 16 12:41:06—Aug 18 12:41:06 UTC	±1.0 days	$(8.0–9.9) \times 10^{-10}$	20–100 keV
NTEGRAL IBIS/ISGRI	Aug 18 12:45:10—Aug 23 03:22:34 UTC	1–5.7 days	2.0×10^{-11}	20–80 keV
INTEGRAL IBIS/ISGRI	Aug 18 12:45:10—Aug 23 03:22:34 UTC	1–5.7 days	3.6×10^{-11}	80–300 keV

Stacked/10 Times Closer

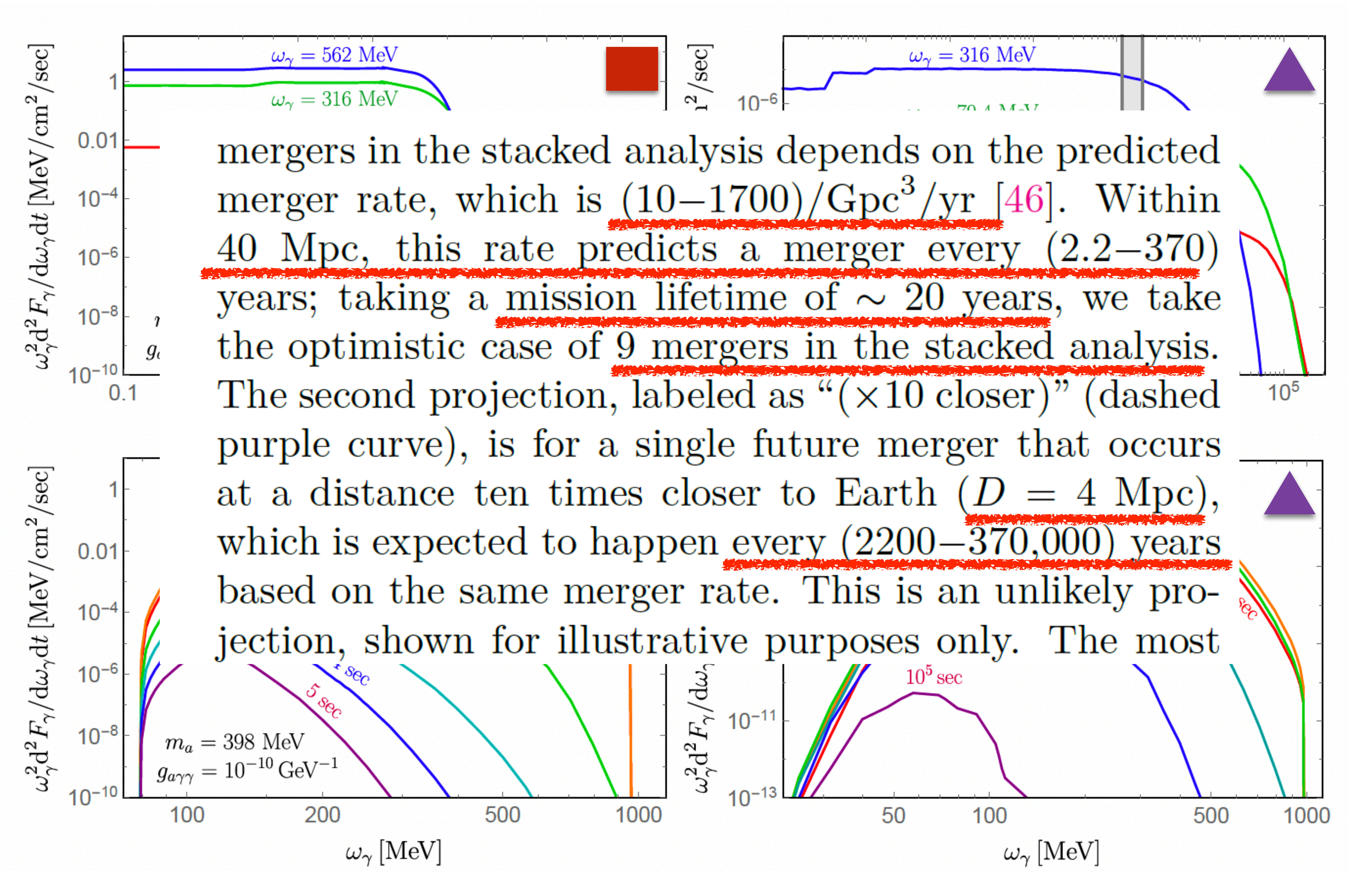

mergers in the stacked analysis depends on the predicted merger rate, which is (10–1700)/Gpc^3/yr [46]. Within 40 Mpc, this rate predicts a merger every (2.2–370) years; taking a mission lifetime of $\sim$ 20 years, we take the optimistic case of 9 mergers in the stacked analysis. The second projection, labeled as "($\times$10 closer)" (dashed purple curve), is for a single future merger that occurs at a distance ten times closer to Earth (D = 4 Mpc), which is expected to happen every (2200–370,000) years based on the same merger rate. This is an unlikely projection, shown for illustrative purposes only. The most

Results

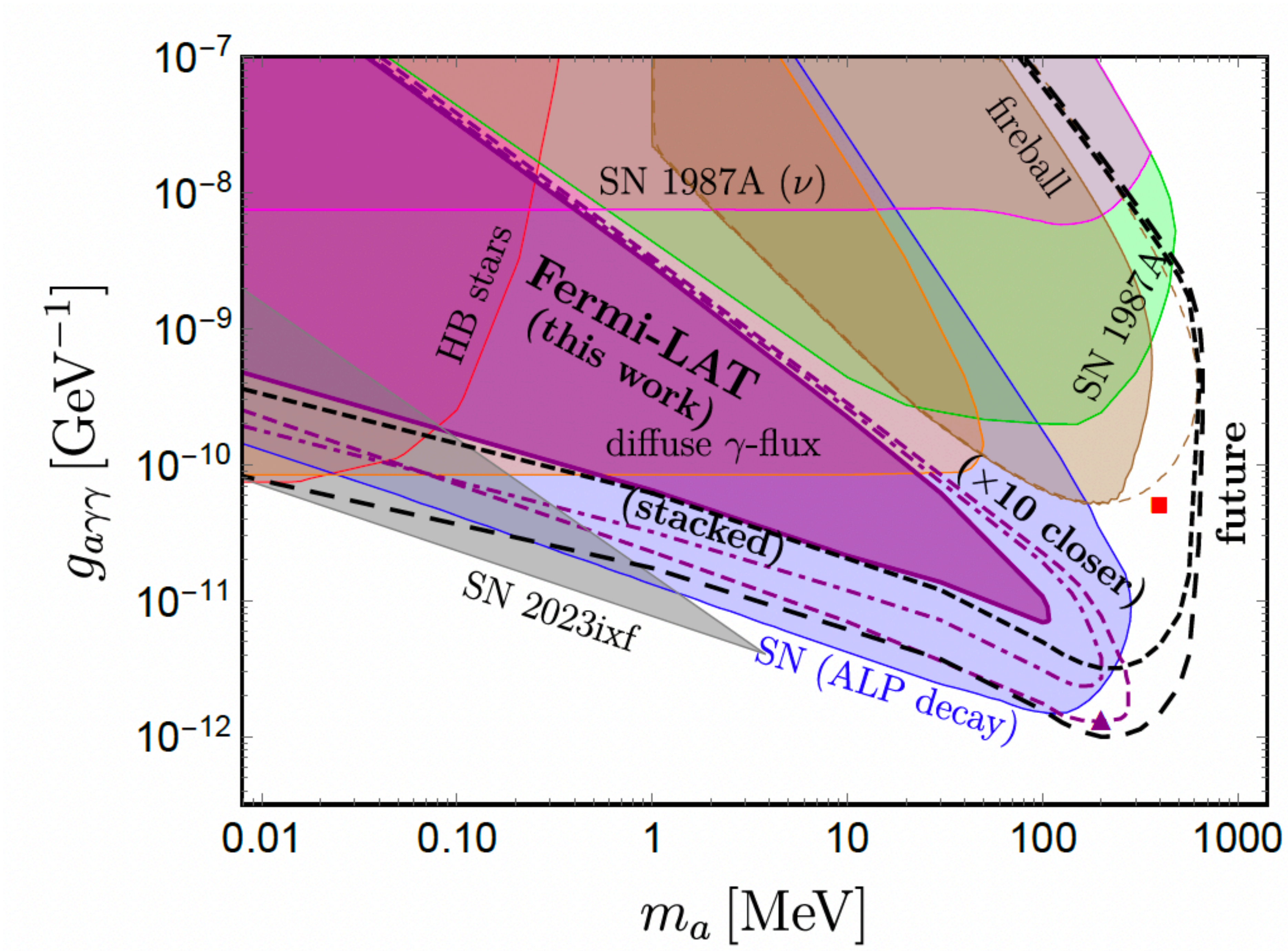

$g_{a\gamma\gamma}$ [GeV^{-1}]
10^{-7}
10^{-8}
10^{-9}
10^{-10}
10^{-11}
10^{-12}
0.01
0.10
1
10
100
1000
m_a [MeV]
SN 1987A (ν)
fireball
HB stars
Fermi-LAT (this work)
SN 1987A
diffuse γ-flux
(stacked)
(×10 closer)
future
SN 2023ixf
SN (ALP decay)

Magnetar/NS Merger Prospects

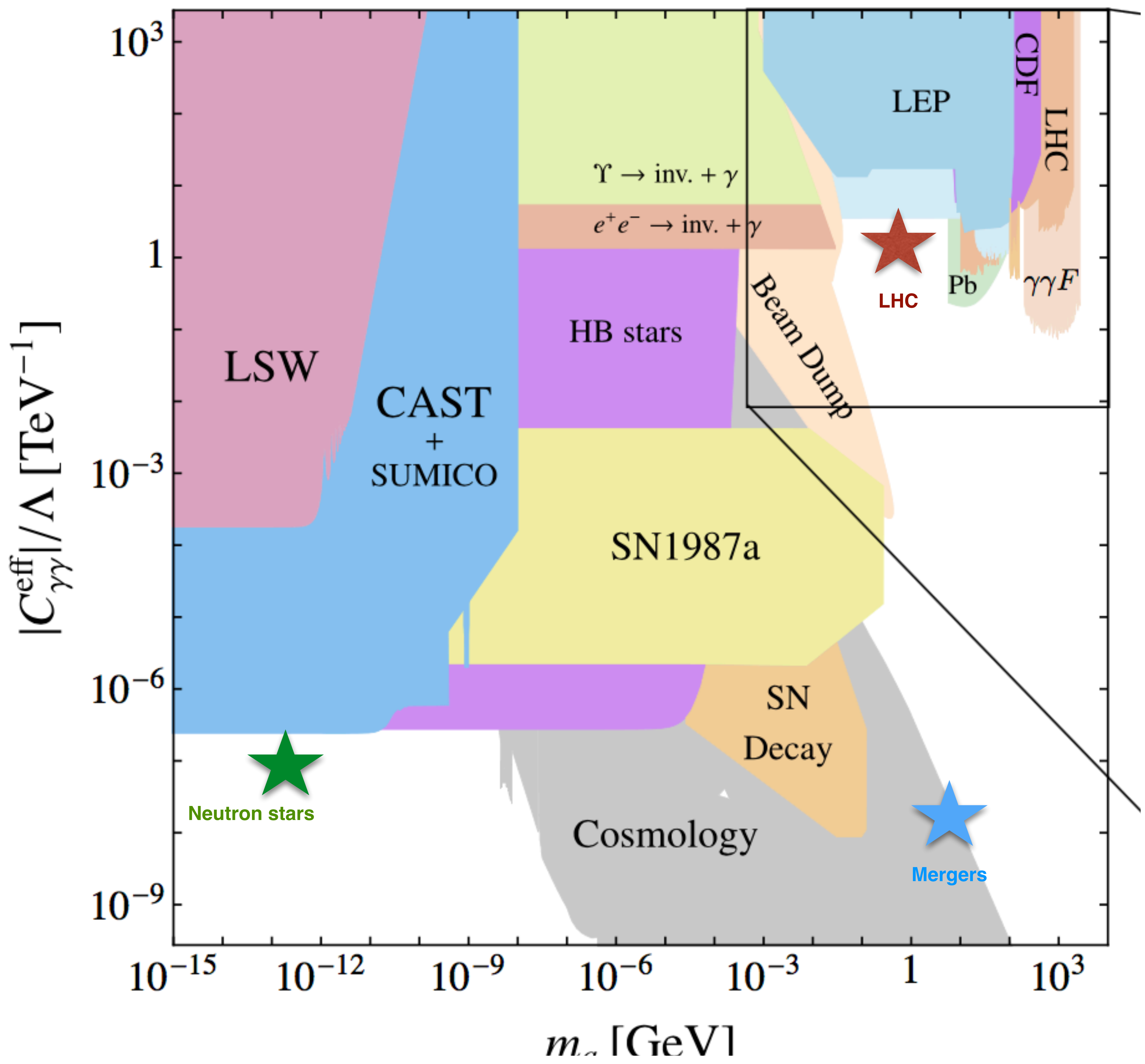

Backup Slides

Production

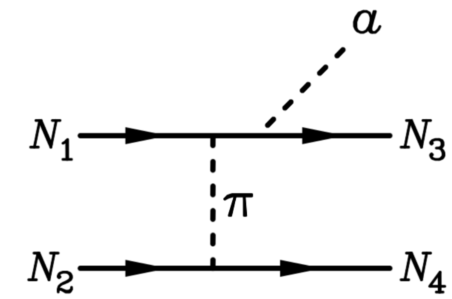
a
N1
N3
π
N2
N4

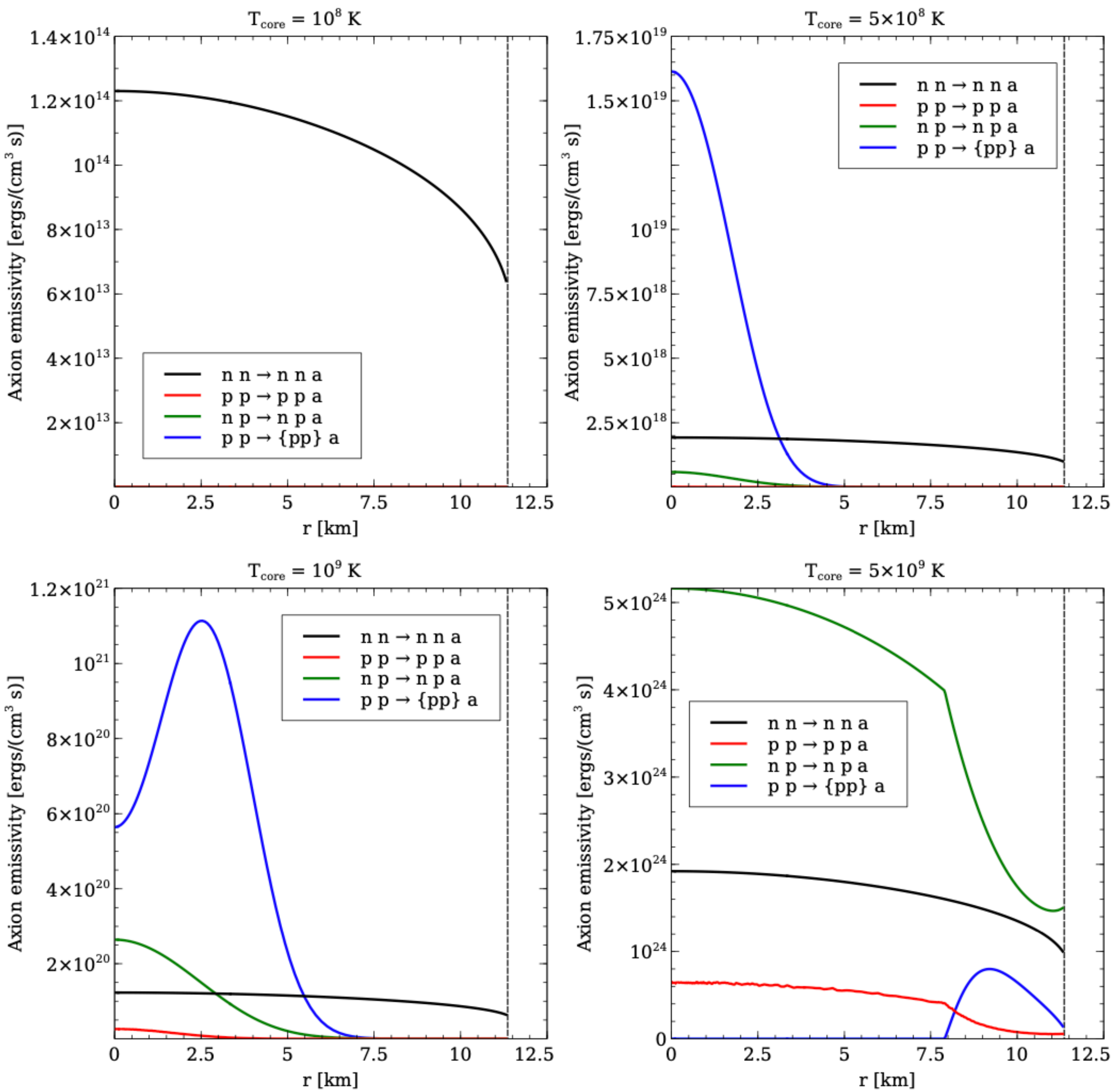
T_core = 10^8 K
T_core = 5×10^8 K
T_core = 10^9 K
T_core = 5×10^9 K
Axion emissivity [ergs/(cm^3 s)]
r [km]
n n → n n a
p p → p p a
n p → n p a
p p → {pp} a

Probe with Supernovae

direction of the SN. There was no statistically significant excess over the background, and hence we can constrain the interaction between heavy ALPs and photons, as was done in e.g. [18, 19, 30]. The ALPs produced in the SN are constrained to induce a photon fluence of $F_\gamma < 1.78\ \mathrm{cm}^{-1}$ at the satellite to be consistent with the (null) observation at the 3 sigma level, or $F_\gamma < 1.19\ \mathrm{cm}^{-1}$ at the 2 sigma level [18].

Muller, Calore, Marsh, et. al. (2023)

SolarMax

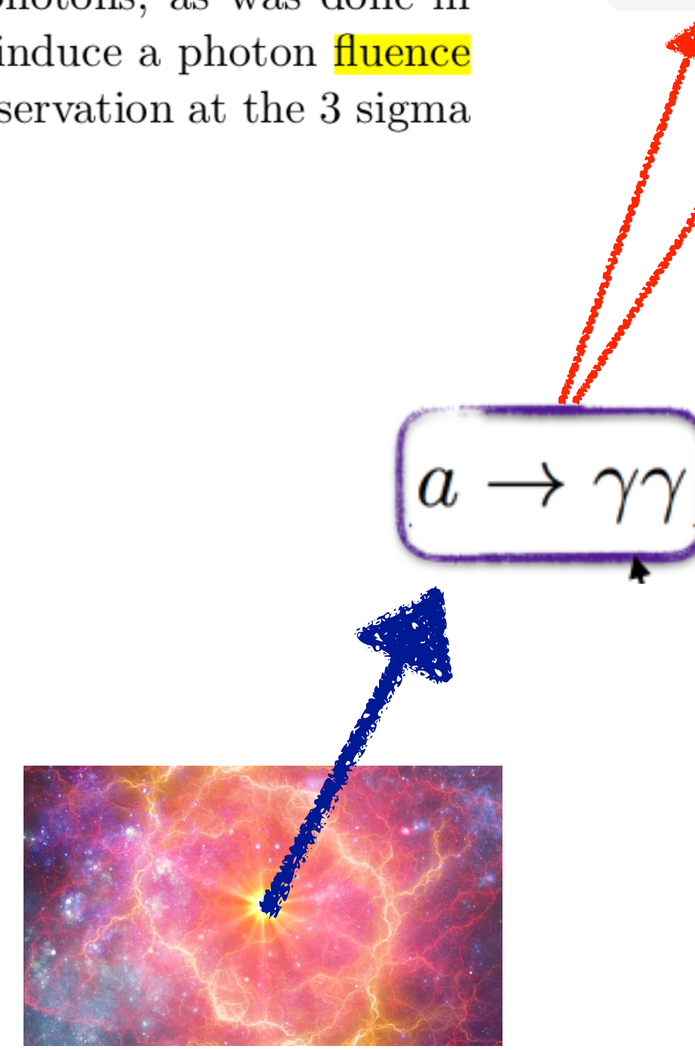

Decay Searches

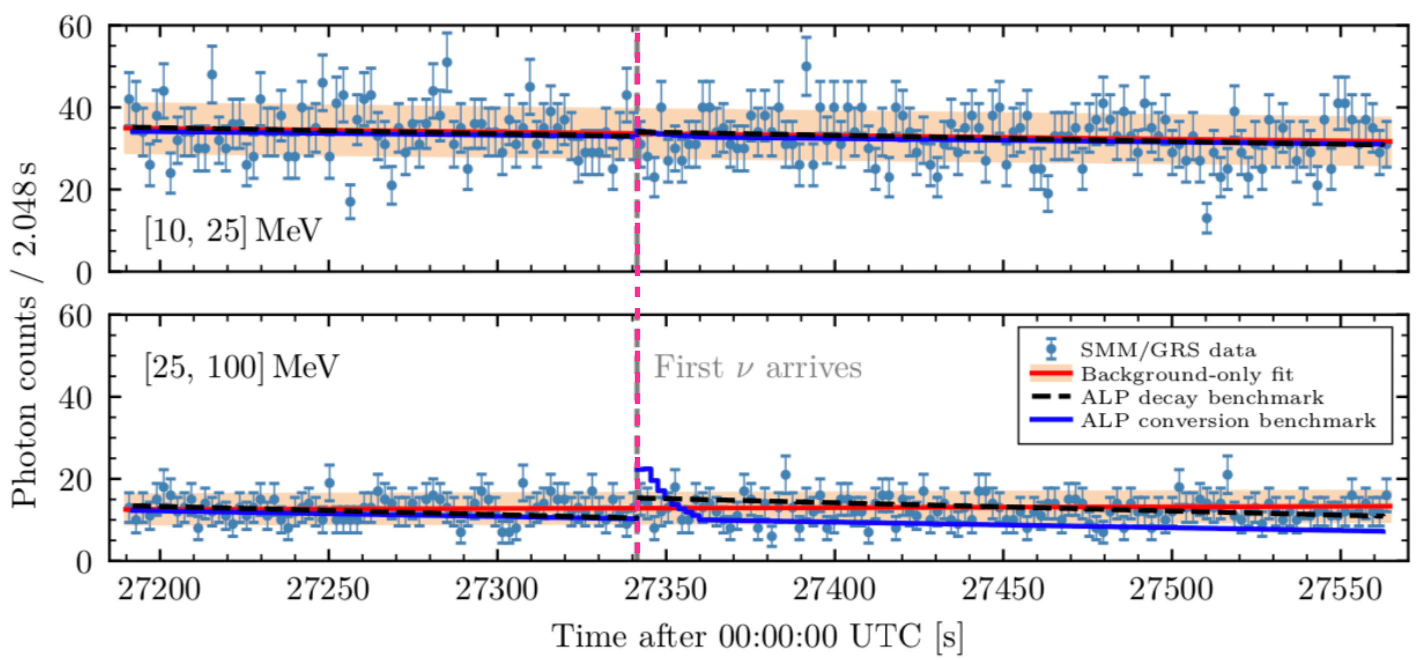

SN 1987A

Hoof, Schulz (2023)

Probe with Supernovae

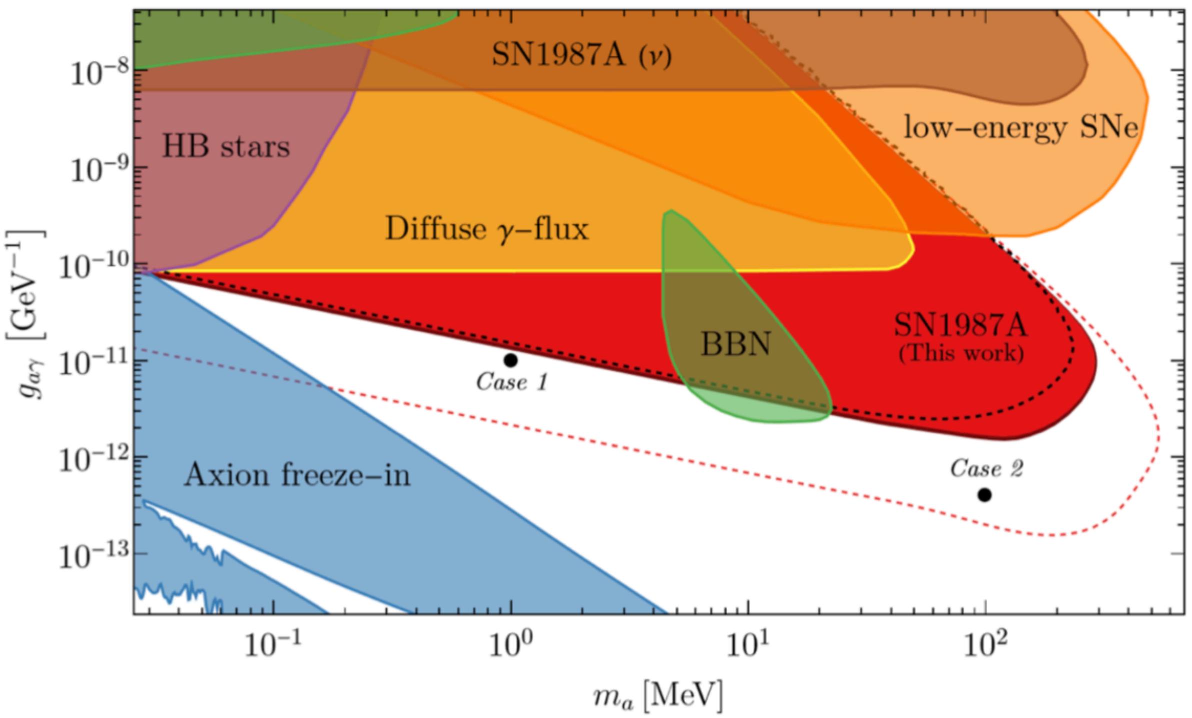

Muller, Calore, Marsh, et. al. (2023)

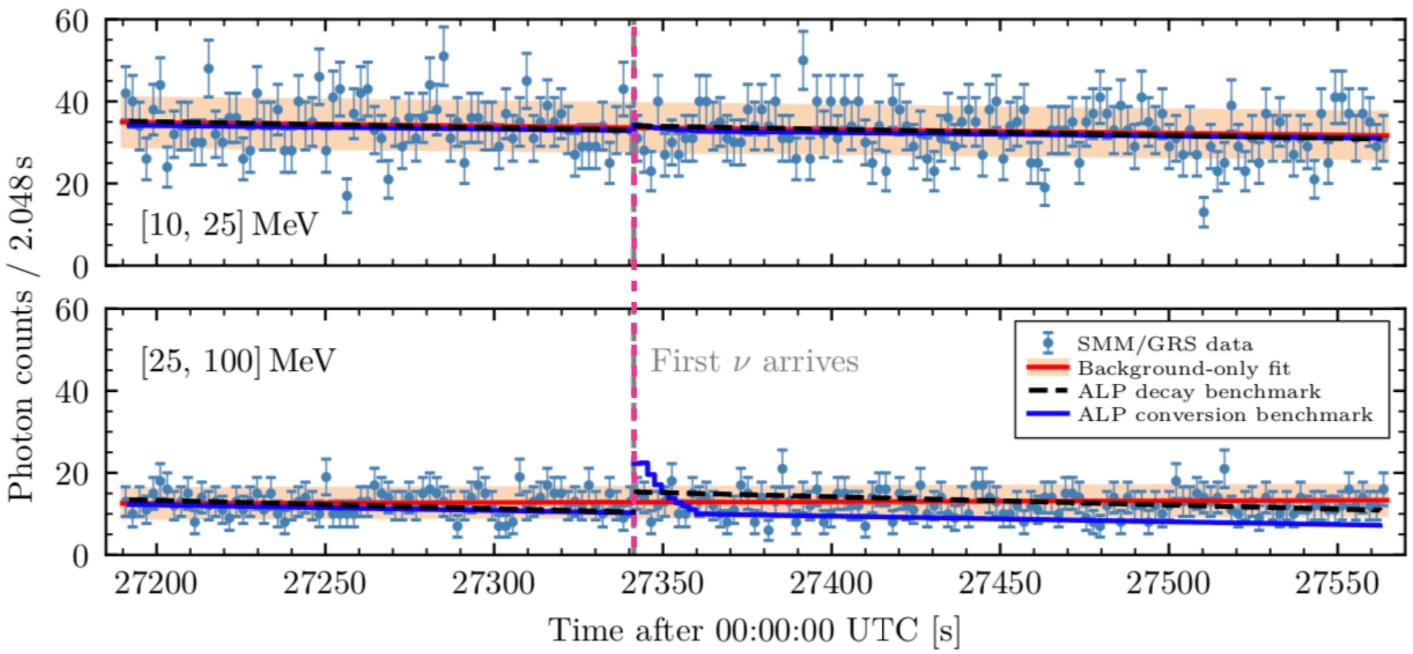

Hoof, Schulz (2023)

SolarMax

$a \to \gamma\gamma$

Decay Searches

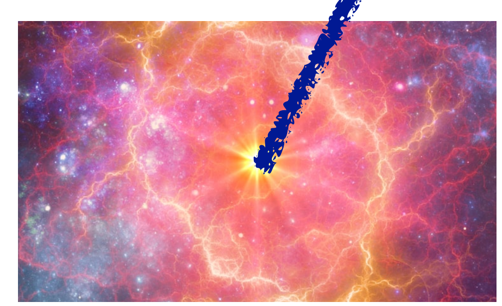

SN 1987A

Conversion Prospects

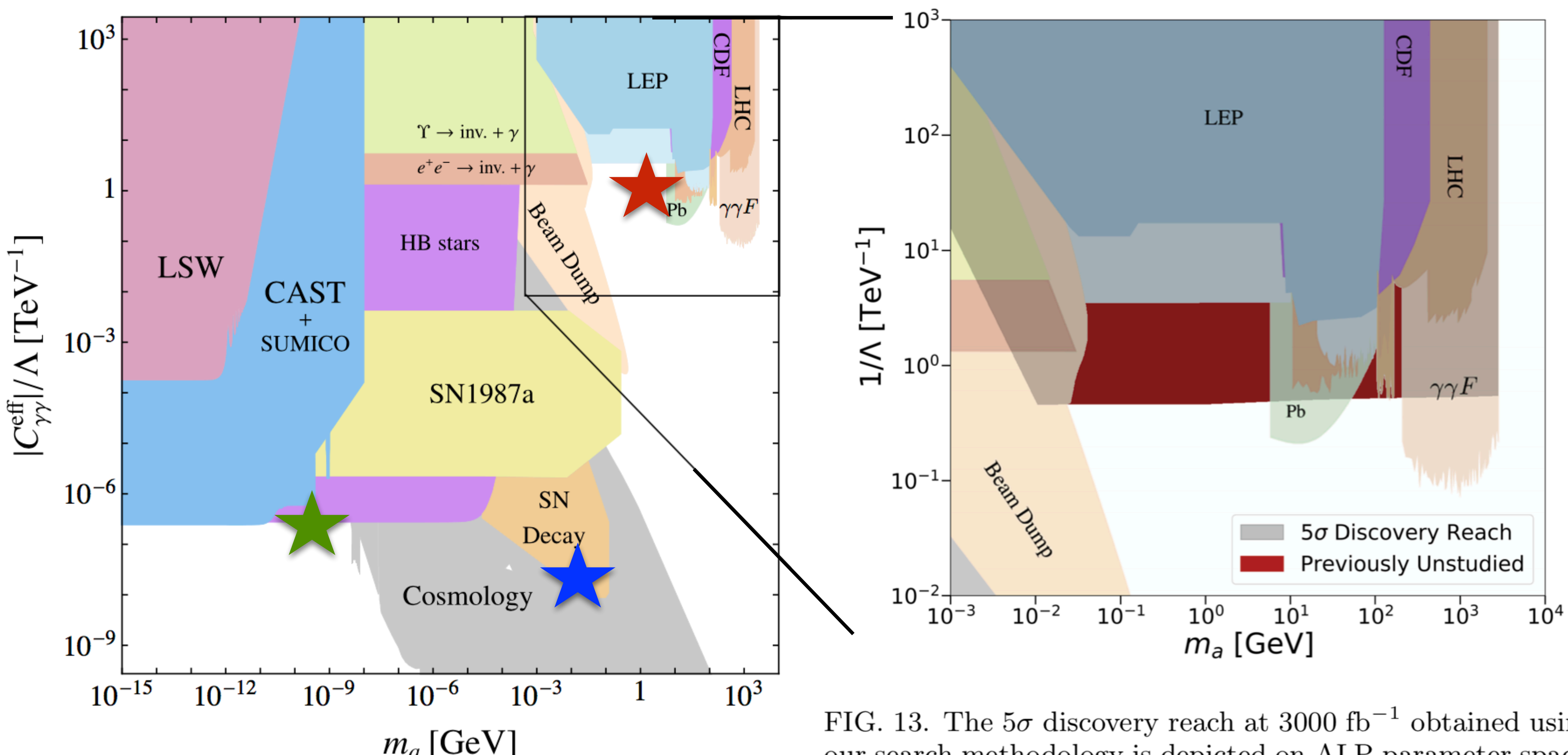

FIG. 13. The 5σ discovery reach at 3000 fb^{-1} obtained using our search methodology is depicted on ALP parameter space, with an emphasis placed on the subset that has previously not been experimentally probed. The other constraints shown are taken from Figure 4 of [31].

A. Gurrola, *KS (2021)*

Conclusions

Supernovae and NS mergers are both interesting

Supernovae: closer, currently stronger bounds

NS mergers: clean timing information

The first second in NS mergers its crucial for BSM

Primakoff in Medium

consider only the two transverse photon modes. The dispersion relation of the transverse modes was calculated in Ref. [68] (see Ref. [1] for a pedagogical discussion). For simplicity, we take the transverse photon dispersion relation to be

$$\omega_\gamma = \sqrt{k^2 + \omega_{\rm pl}^2}\,, \tag{S1}$$

(k being the photon momentum) where the photon essentially has a mass equal to the plasma frequency $\omega_{\rm pl}$ of the medium. This approximation is common in the literature [45, 69–76]. In NS merger or supernovae conditions, the plasma frequency is dominated by the most mobile species of particles possessing electric charge, which in this case are the strongly degenerate and ultrarelativistic electrons. The plasma frequency is given by [68]

$$\omega_{\rm pl} = \sqrt{\frac{4\alpha}{3\pi}\left(\mu_e^2 + \frac{\pi^2}{3}T^2\right)}\,, \tag{S2}$$

In a plasma, the electromagnetic interaction is screened by the motion of charged particles. Screening in the hot, dense matter in a merger remnant is likely dominated by the nondegenerate protons [1], leading to a Debye screening scale

$$k_S = 2\sqrt{\frac{\alpha\pi n_p}{T}}\,, \tag{S3}$$

Primakoff in Medium

Without correlations, the squared matrix element involves $|\mathbf{q}|^{-4}$ from the Coulomb propagator. In order to account for screening effects one should substitute

$$|\mathbf{q}|^{-4} \to |\mathbf{q}|^{-4}\, S(\mathbf{q}) \qquad\qquad S(\mathbf{q}) = \frac{\mathbf{q}^2}{\mathbf{q}^2 + k_{\mathrm{S}}^2} \tag{6.71}$$

for the structure factor.

$$\frac{1}{|\mathbf{q}|^4} \to \frac{1}{\mathbf{q}^2\,(\mathbf{q}^2 + k_{\mathrm{S}}^2)} \tag{6.72}$$

in the weak-screening limit (Debye screening).

Primakoff in Medium

The Primakoff process, depicted in the left panel of Fig. S1, involves the conversion of a photon to an ALP through electromagnetic scattering. We shall consider only scattering with protons $\gamma + p \to a + p$ and not with electrons $\gamma + e^- \to a + e^-$, because the electron population is strongly degenerate, which suppresses that scattering rate. The matrix element for the Primakoff process $\gamma(p_2) + p(p_1) \to a(p_4) + p(p_3)$ reads

$$-i\mathcal{M} = \bar{u}(p_3)\left(i\sqrt{4\pi\alpha}\gamma^\mu\right)u(p_1)\left(\frac{-ig_{\mu\nu}}{q^2}\right)\left[-ig_{a\gamma\gamma}\varepsilon^{\alpha\nu\rho\sigma}q_\rho p_{2\sigma}\varepsilon_\alpha(p_2)\right]. \tag{S4}$$

Summing over spins and the two transverse polarizations of the photon $\sum_{\text{pol}}\varepsilon_\alpha\varepsilon^*_\gamma \to -g_{\alpha\gamma}$, one ends up with the squared matrix element

$$\sum_{\text{spin, pol}}|\mathcal{M}|^2 = \frac{32g^2_{a\gamma\gamma}\pi\alpha}{q^4}\Big[m_p^2 m_\gamma^2 q^2 - m_p^2(p_2\cdot q)^2 - m_\gamma^2(p_1\cdot q)(p_3\cdot q) - q^2(p_1\cdot p_2)(p_2\cdot p_3) + (p_1\cdot q)(p_2\cdot q)(p_2\cdot p_3) + (p_2\cdot q)(p_3\cdot q)(p_1\cdot p_2)\Big]. \tag{S5}$$

$$\sum_{\text{spin,pol}}|\mathcal{M}|^2 = \frac{32g^2_{a\gamma\gamma}\pi\alpha m_p^2}{\mathbf{q}^4}\left[\mathbf{p_2}^2\mathbf{p_4}^2 - (\mathbf{p_2}\cdot\mathbf{p_4})^2\right] = \frac{32g^2_{a\gamma\gamma}\pi\alpha m_p^2}{\mathbf{q}^4}|\mathbf{p_2}\times\mathbf{p_4}|^2. \tag{S8}$$

From this matrix element, one can derive the cross section given in Ref. [1].

To get the ALP production spectrum, we now integrate this squared matrix element over the phase space:

$$\Gamma = \int\frac{d^3p_1}{(2\pi)^3}\frac{d^3p_2}{(2\pi)^3}\frac{d^3p_3}{(2\pi)^3}\frac{d^3p_4}{(2\pi)^3}(2\pi)^4\delta^4(p_1+p_2-p_3-p_4)\frac{32g^2_{a\gamma\gamma}\pi\alpha m_p^2}{\mathbf{q}^4}\frac{\left[\mathbf{p_2}^2\mathbf{p_4}^2-(\mathbf{p_2}\cdot\mathbf{p_4})^2\right]}{16E_1E_2E_3E_4}f_1g_2(1-f_3), \tag{S9}$$

where f represents the Fermi-Dirac distribution of the proton and g the Bose-Einstein distribution of the photon.

Photon Fusion in Medium

In medium, as well as in vacuum, ALPs can be produced through photon coalescence, as shown in the right panel of Fig. S1. We calculate the rate of ALP production from photon coalescence, taking into account the in-medium photon properties. The squared matrix element for $\gamma + \gamma \to a$ is

$$\sum |\mathcal{M}|^2 = \frac{1}{2} g_{a\gamma\gamma}^2 m_a^2 (m_a^2 - 4m_\gamma^2) \,. \tag{S18}$$

The rate of photon coalescence $\gamma + \gamma \to a$ is given by the phase space integral

$$\Gamma = \int \frac{\mathrm{d}^3 p_1}{(2\pi)^3} \frac{\mathrm{d}^3 p_2}{(2\pi)^3} \frac{\mathrm{d}^3 p_a}{(2\pi)^3} (2\pi)^4 \delta^4(p_1 + p_2 - p_a) \frac{\frac{1}{4} g_{a\gamma\gamma}^2 m_a^2 \left(m_a^2 - 4m_\gamma^2\right)}{2^3 E_1 E_2 E_a} g_1 g_2 \,, \tag{S19}$$

where g_1 and g_2 are Bose-Einstein distributions for the two incoming photons. Again, we neglect the Bose enhancement factor for the ALPs because we only consider ALPs that couple weakly enough to free-stream through the system.

Probe with Neutron Stars

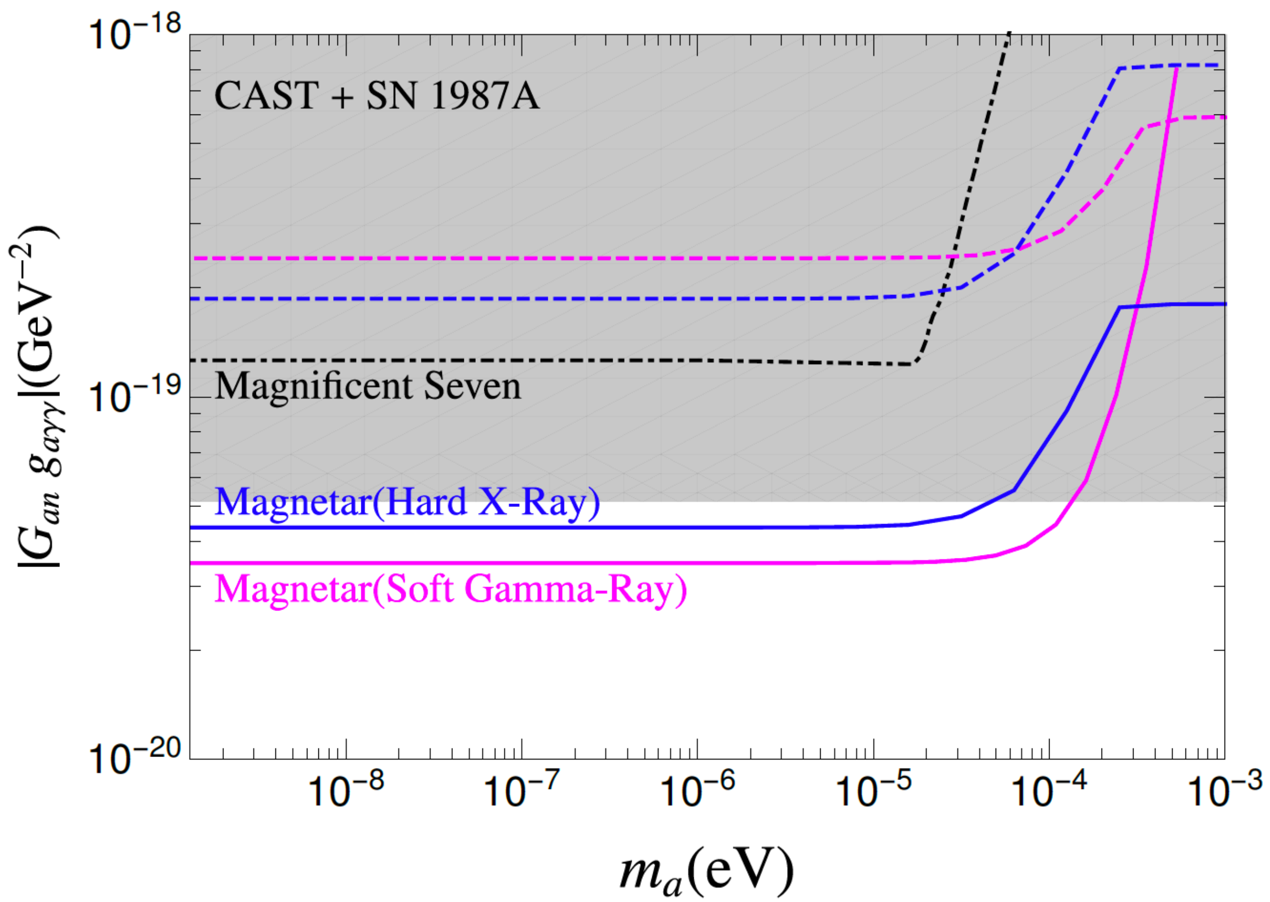

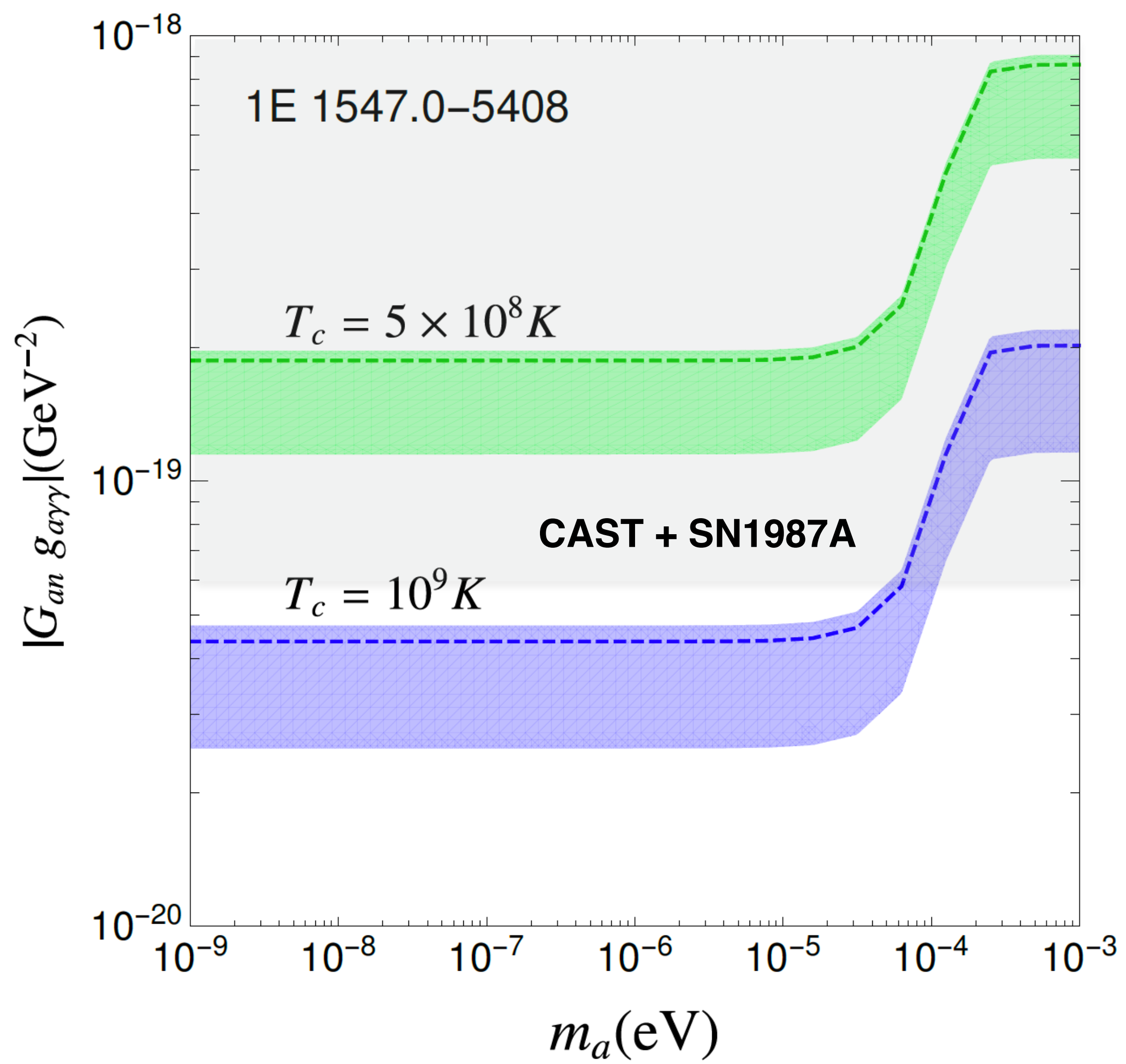

Axion spectrum emitted from a neutron star with matter modeled by the IUF EoS and with $^1S_0$ CCDK proton superfluidity, for different choices of the neutron star mass. ***Top right***

two choices of core temperature and with the band representing the uncertainty in $dN_a / d\omega$ due to uncertainties in the nuclear EoS, the magnetar mass, and the critical temperature of proton $^1S_0$ proton pairing. The dashed curves correspond to the choices (IUF, $1.4M_\odot$, CCDK).

Fortin, Guo, Harris, Sheridan, KS (2021)

Light Scalars in Neutron Star Mergers

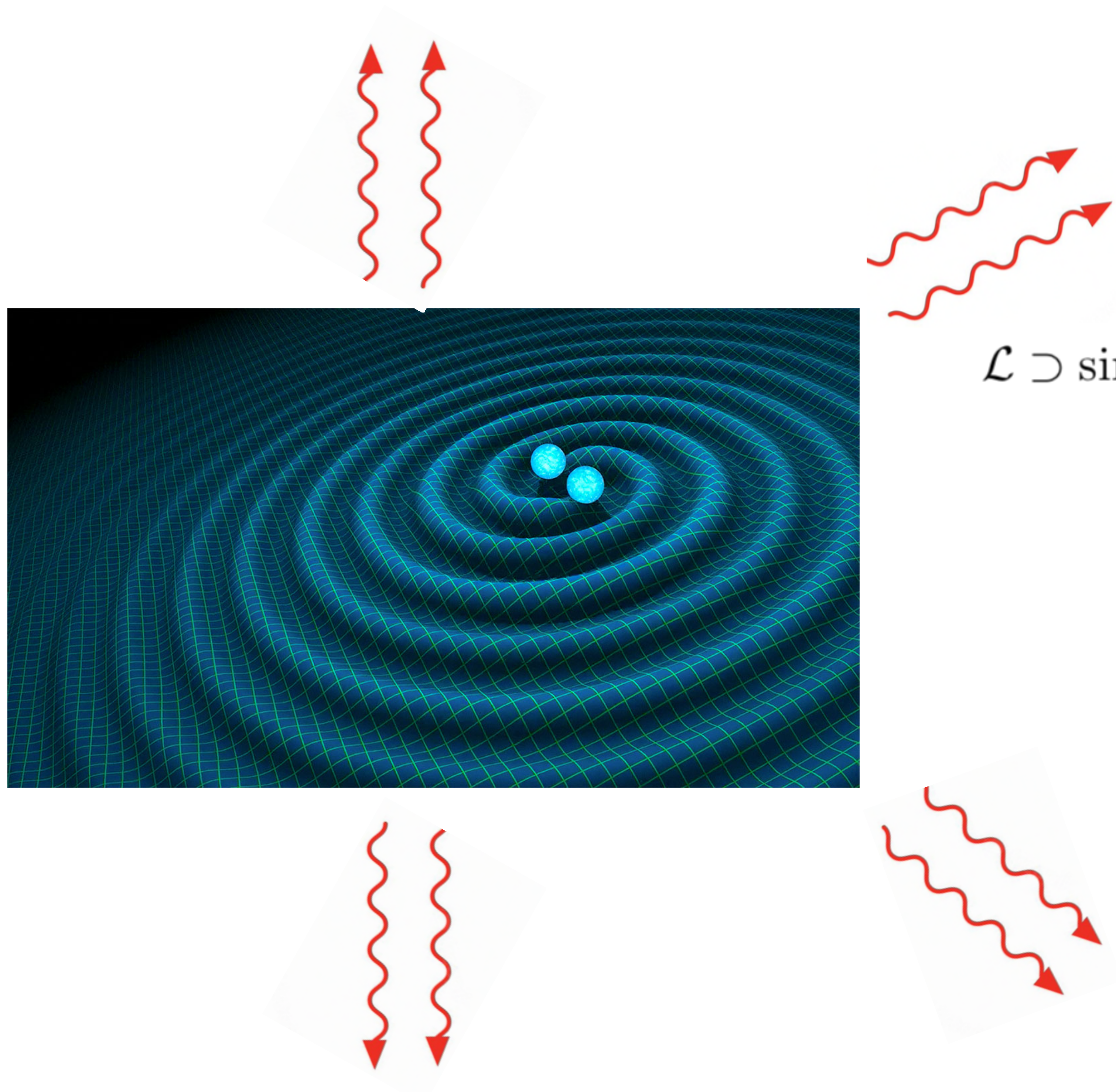

$$\mathcal{L} \supset \sin\theta \left[y_{hNN} S \bar{N} N + A_\pi (S \pi^0 \pi^0 + S \pi^+ \pi^-) \right]$$

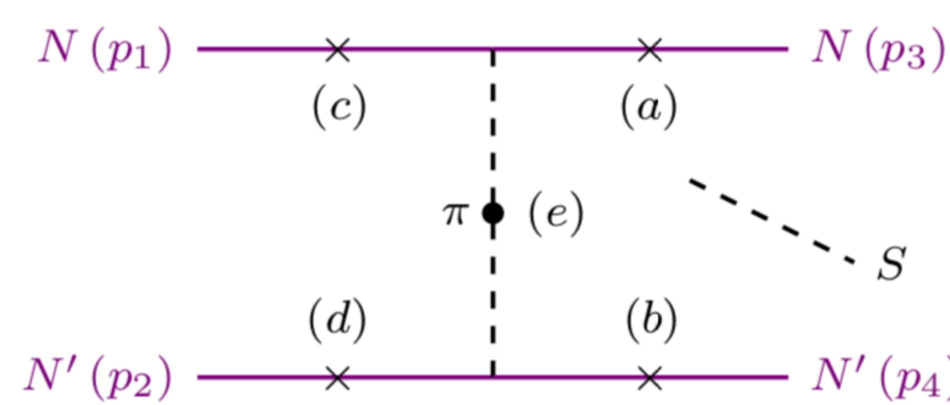

Nucleon bremsstrahlung

JHEP 04 (2019) 052

JCAP 07 (2020) 023

Dev, Harris, Fortin, *KS*, Zhang